

A GIS Pipeline to produce GeoAI Datasets from Drone Overhead Imagery

Professor John R. Ballesteros

PhD. Informatics, UNC

MS GeonInformatics, ITC, The Netherlands

Geologist

jballes@unal.edu.co

Agenda

- GeoAI
- Machine Learning and Deep Learning
- GeoAI Datasets
- Applications
- A GIS Pipeline for GeoAI datasets
- A road dataset example for semantic segmentation
- Learning Test

GeoAI

A set of techniques at the intersection of AI and Geospatial Analysis for geographic knowledge discovery.

(Janowicz et al., 2019)

Machine Learning

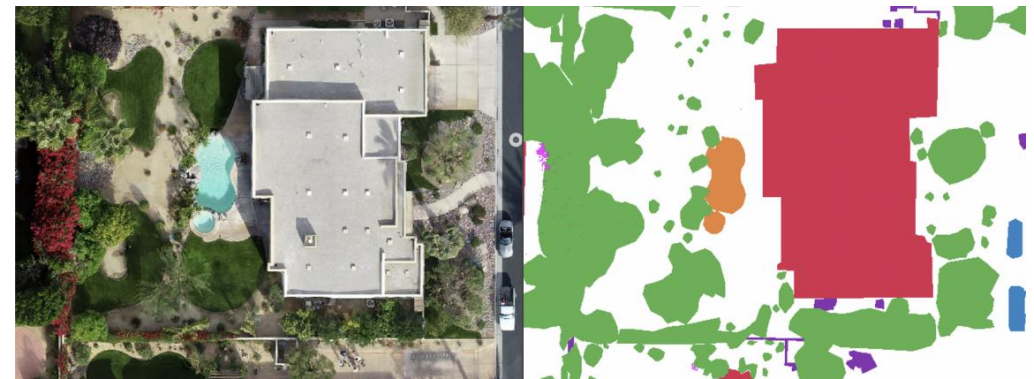
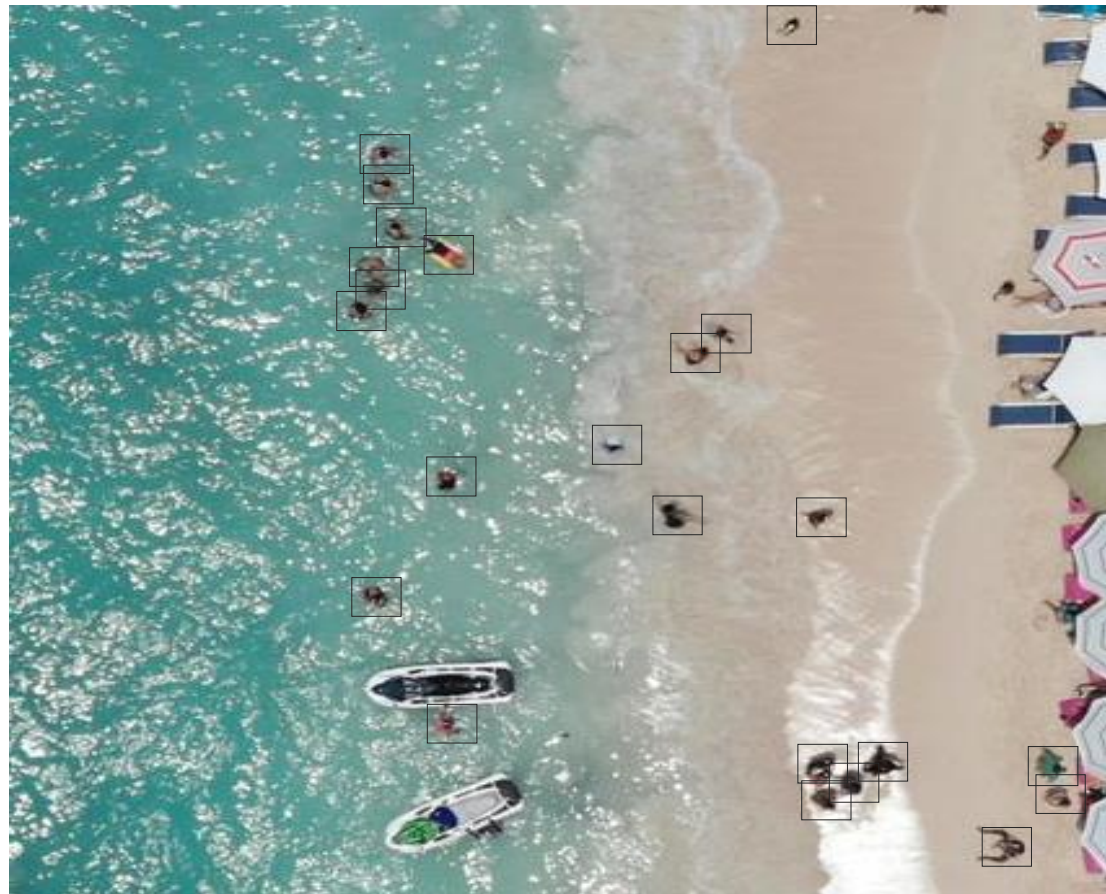
Algorithms that learn directly from data instead of being explicitly programmed.

Deep Learning

Uses mapping function created by layers of neurons emulating how the brain Works.

GeoAI Datasets

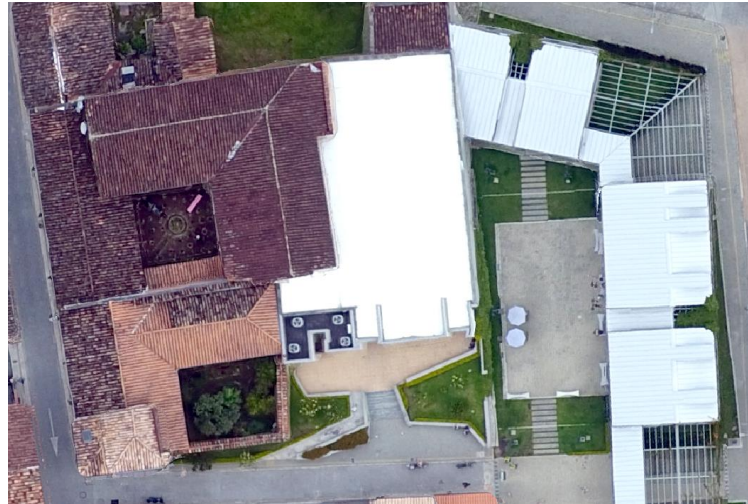
Unbiased and enhanced data features



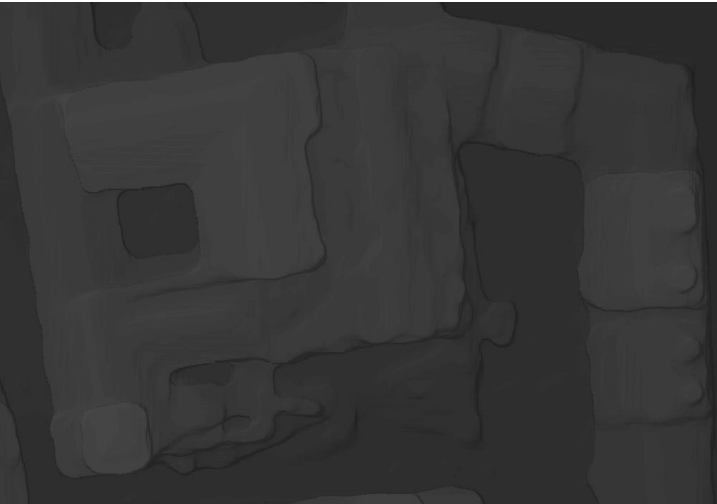
(Blaga and Nedevschi., 2020)



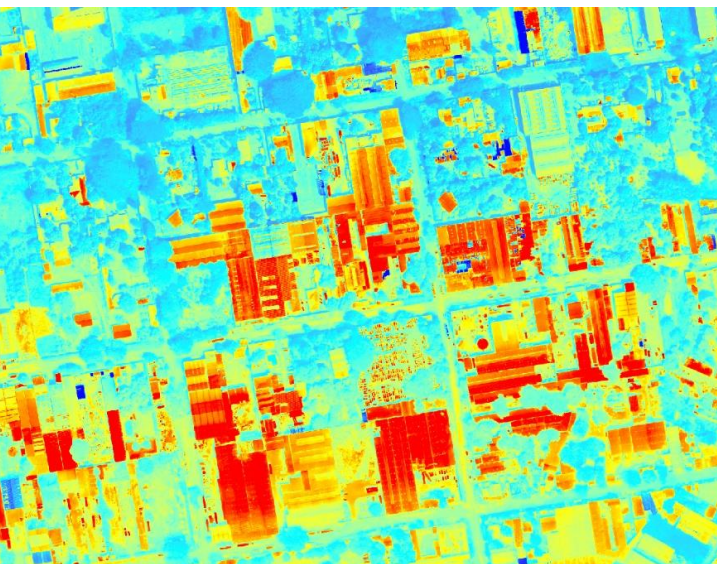
RGB



LIDAR



NIR



SAR

THERMAL

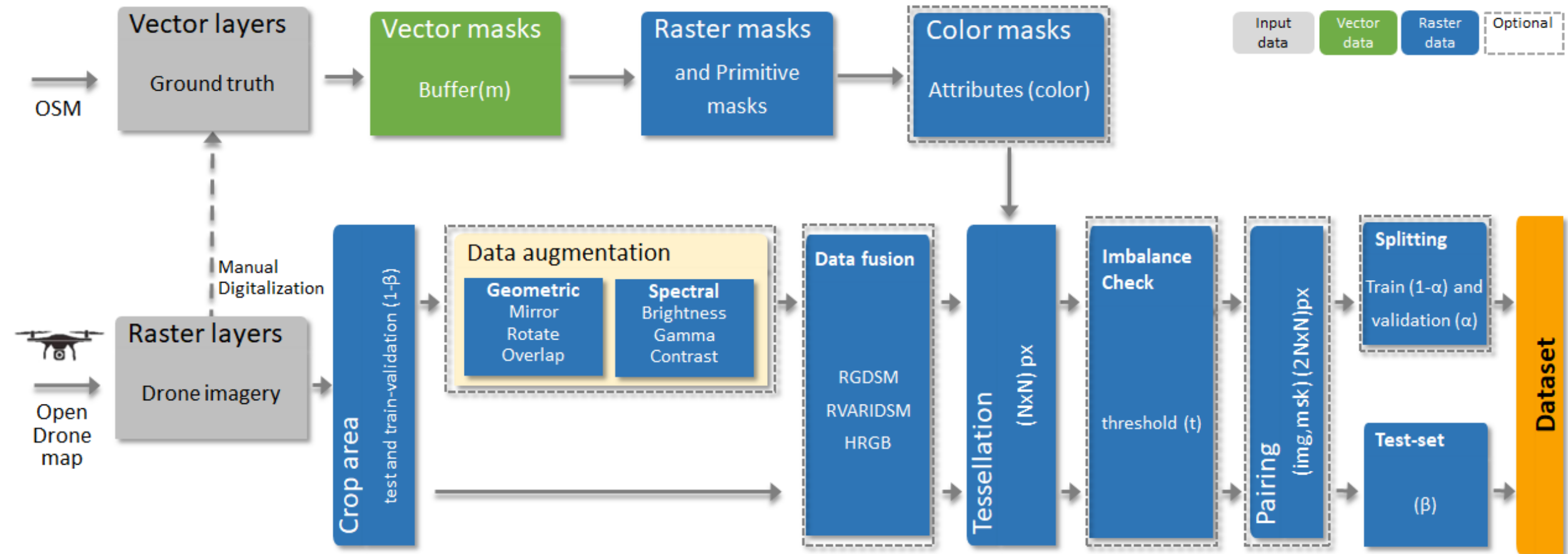
RG-DSM

Applications

Encompassing the fast and increasing acquisition of aerial-drone-satellite imagery with the spatial analysis and map production for :

- ***Mapping & cartography*** (in minutes nor months).
- ***Cadaster***
- ***Logistics and Routing***
- ***Disaster management*** (quick production of maps is needed)
- ***Oil and Gas***
- ***Solar Energy***
- ***Urban Planning***
- ***Current environmental problems: Heat Islands***

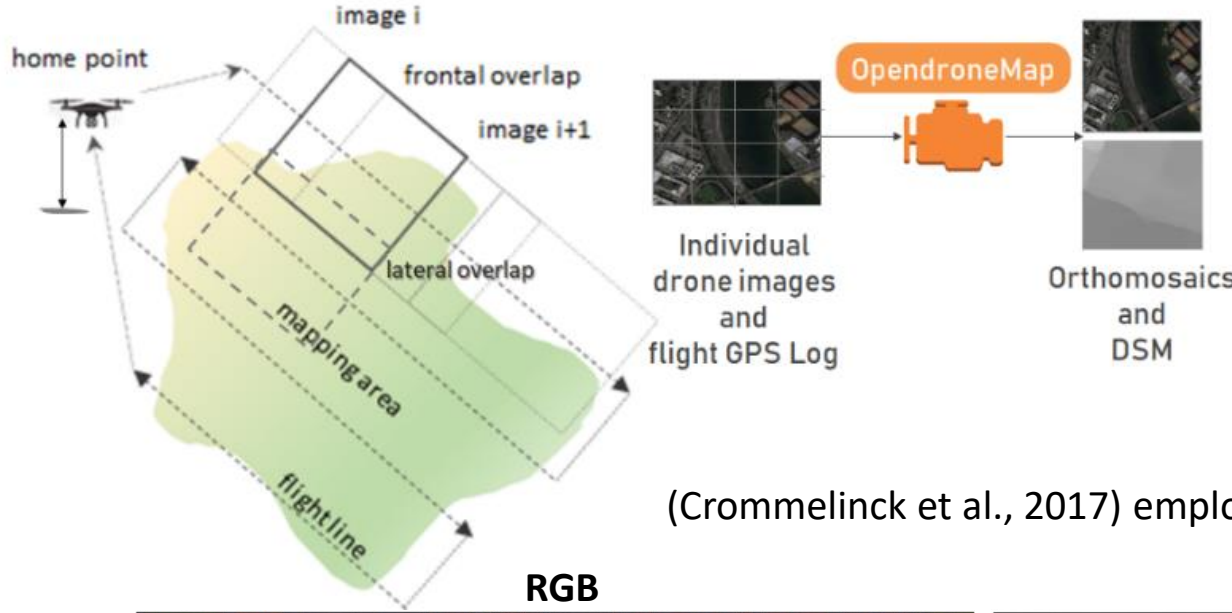
Proposed GIS Pipeline to Produce GeoAI Datasets from Drone Overhead Imagery



Ballesteros, John R., German Sanchez-Torres, and John W. Branch-Bedoya. 2022. "A GIS Pipeline to Produce GeoAI Datasets from Drone Overhead Imagery" *ISPRS International Journal of Geo-Information* 11, no. 10: 508. <https://doi.org/10.3390/ijgi11100508>

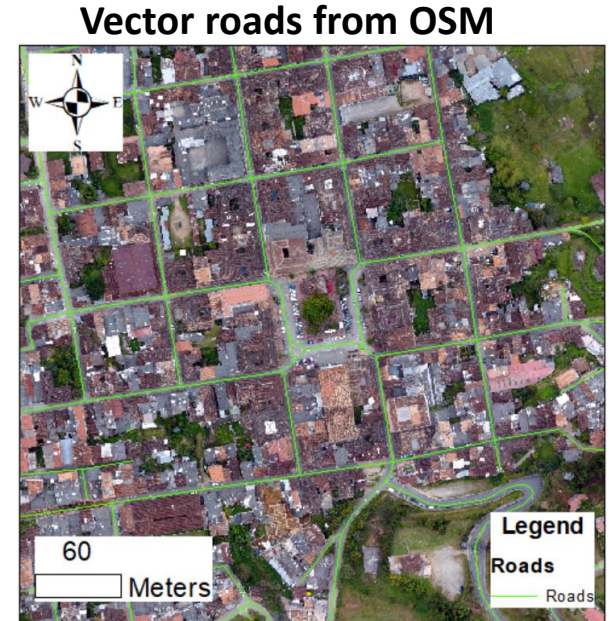
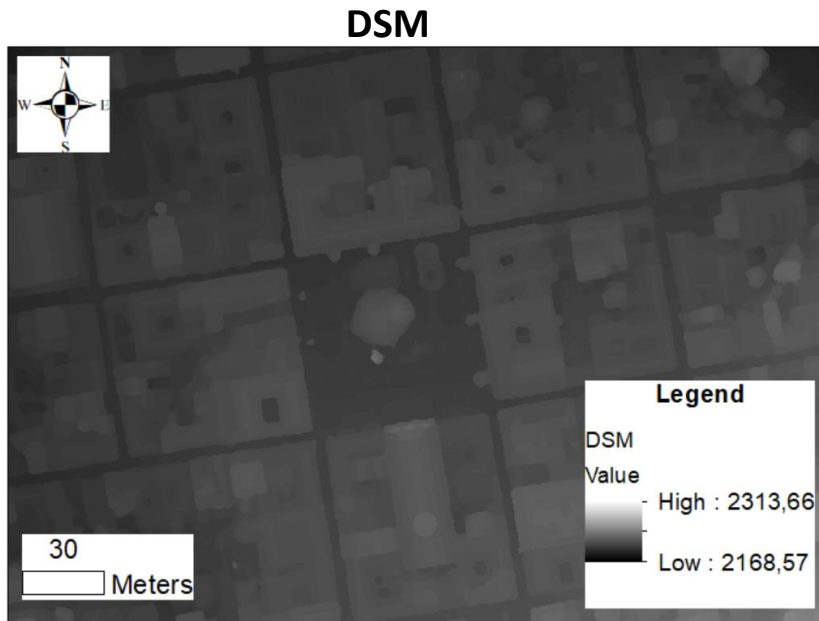
Drone Imagery Acquisition & Orthomosaic Production

Automatic flight

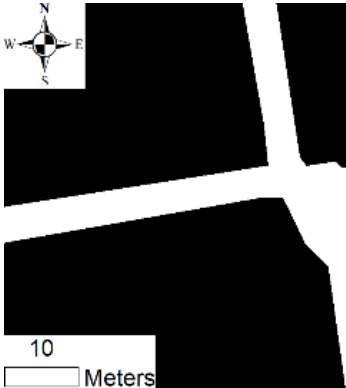


See
For an example of the result

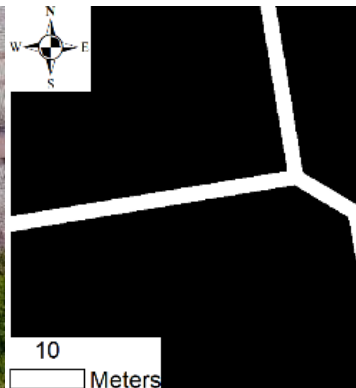
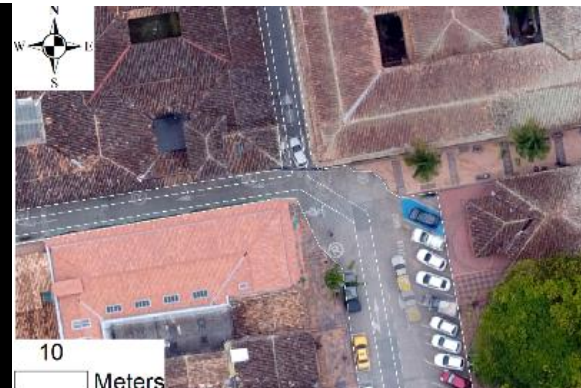
(Crommelinck et al., 2017) employed opendronemap for UAV imagery acquisition for cadaster.



Type of Masks



Full-size mask

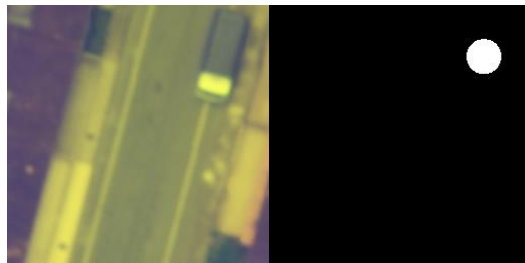


Equal-size mask



Color mask

Primitive-mask the simplest raster representation of objects present in input images that allow models to learn objects' structure and simplify their vectorization



(Image, Point primitive-mask), ex. Vehicles

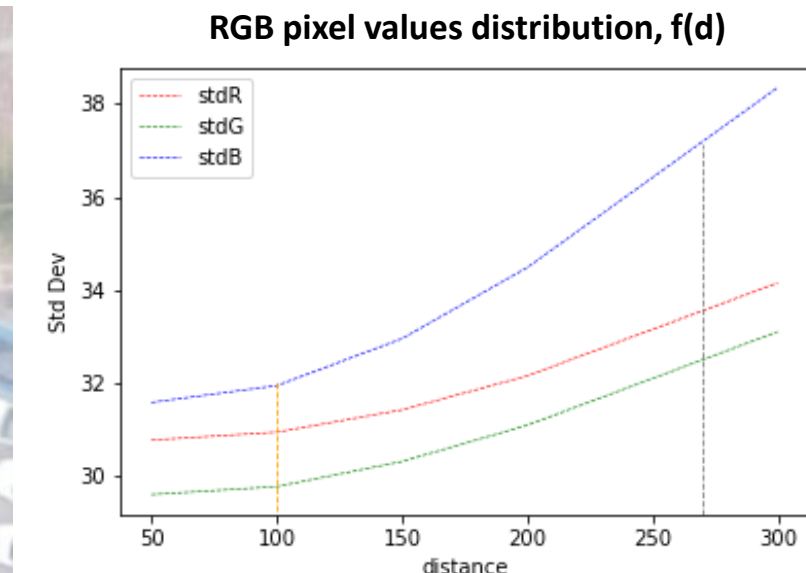
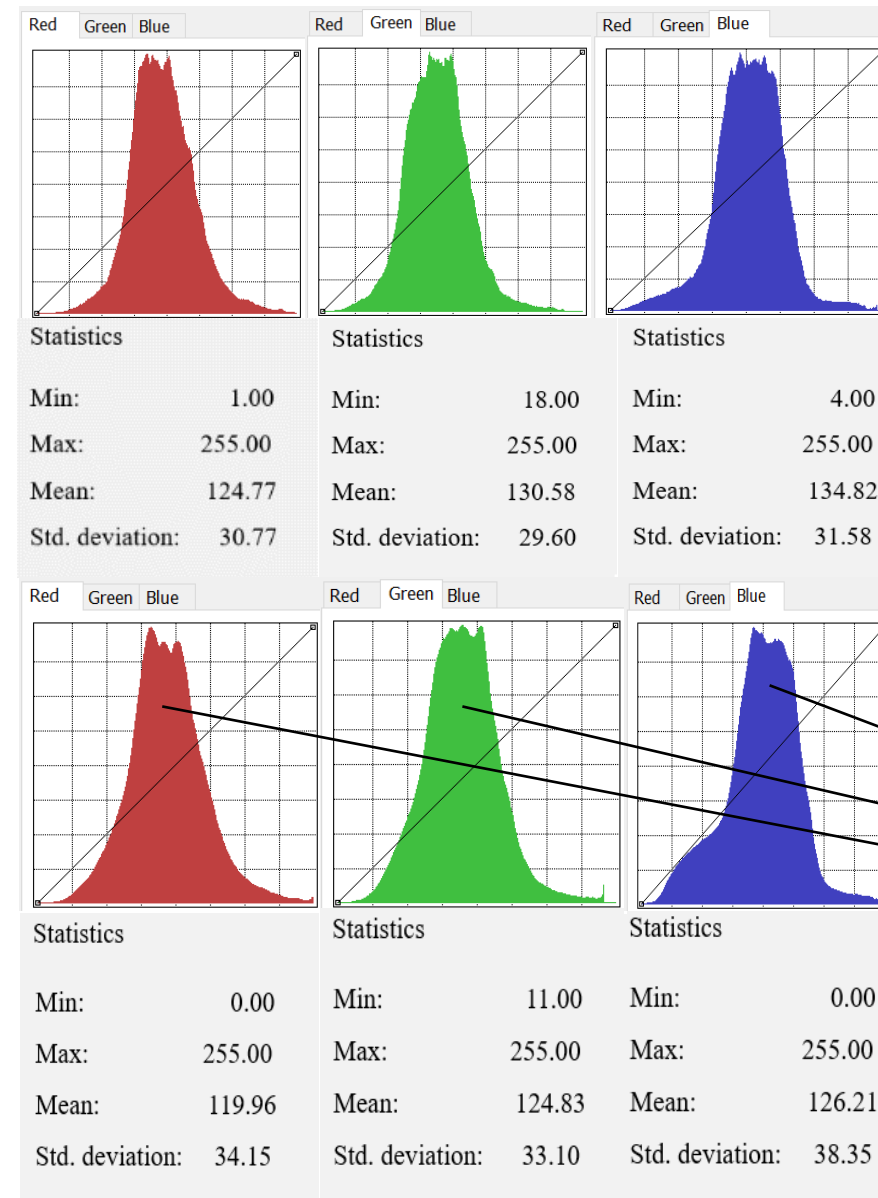


(Image, Line primitive-mask), ex. Roads



(Image, Polygon primitive-mask), ex. Buildings

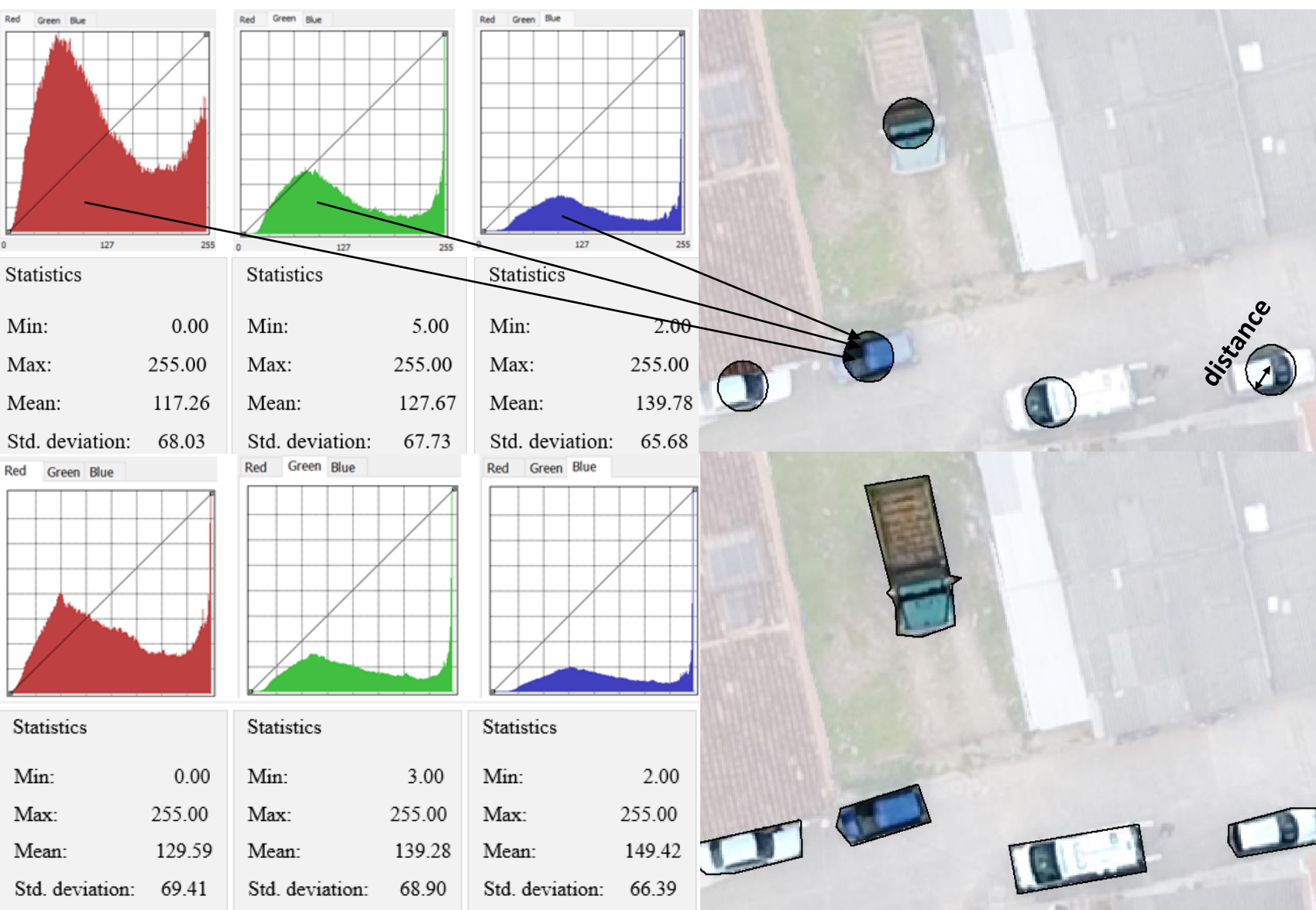
Producing Primitive Linear Masks



Buffer distance of masks and RGB pixel distribution

Ballesteros, J.R.; Sanchez-Torres, G.; Branch-Bedoya, J.W., 2022

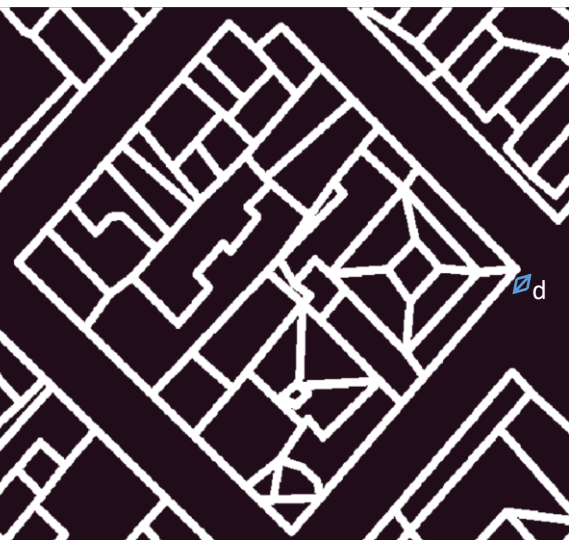
Producing Primitive Point Masks



Buffer distance of masks and RGB pixel distribution

Ballesteros, J.R.; Sanchez-Torres, G.; Branch-Bedoya, J.W., 2022

Producing Primitive Polygon Masks



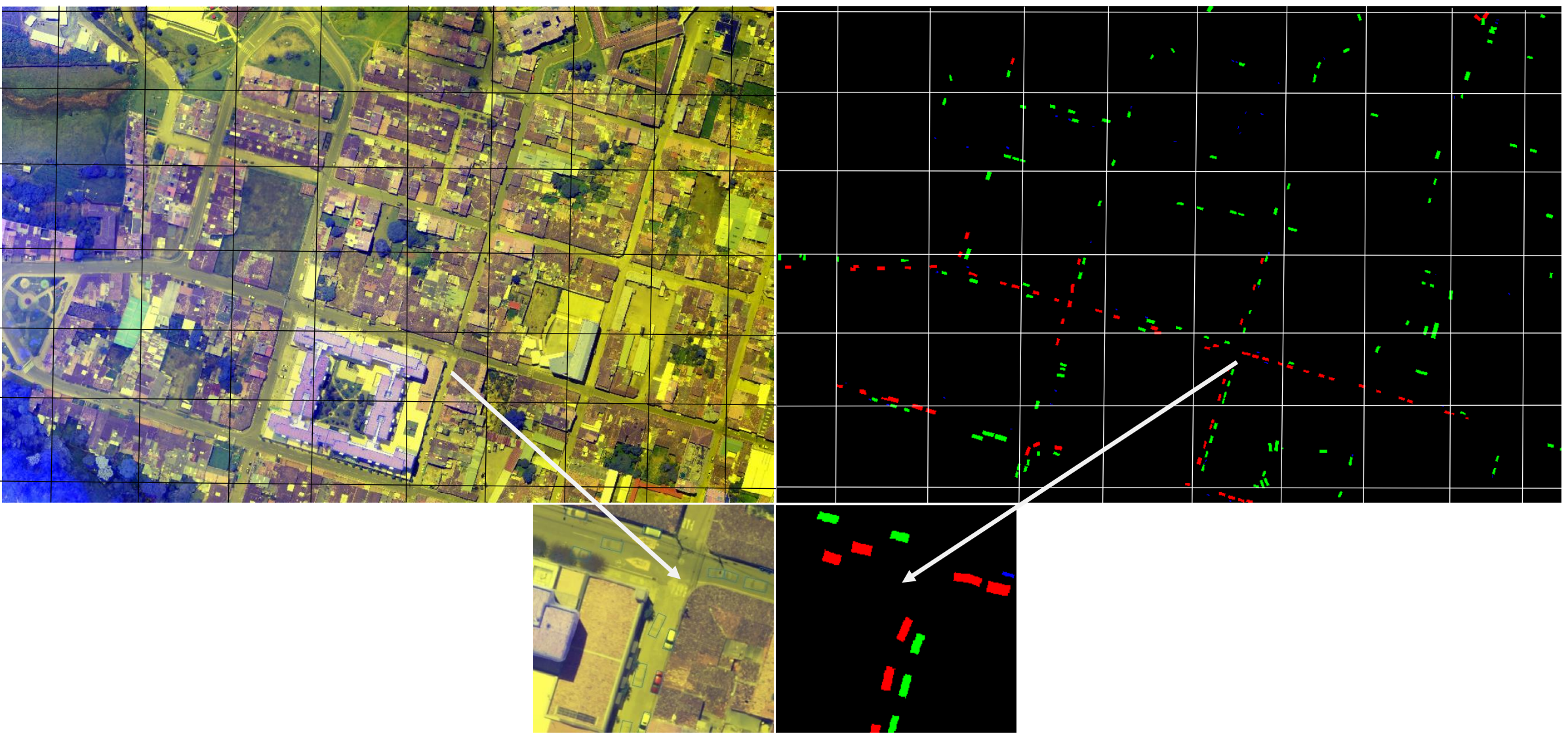
- **Massachusetts Building Dataset**
- Mnih et al, 2013

RID Dataset (A boundary mask dataset)

Ballesteros, Sanchez-

Torres, Branch-Bedoya, 2022 in progress

- High resolution
- Describes roof structure (runoff, material and area)
- High density building areas (developing countries)



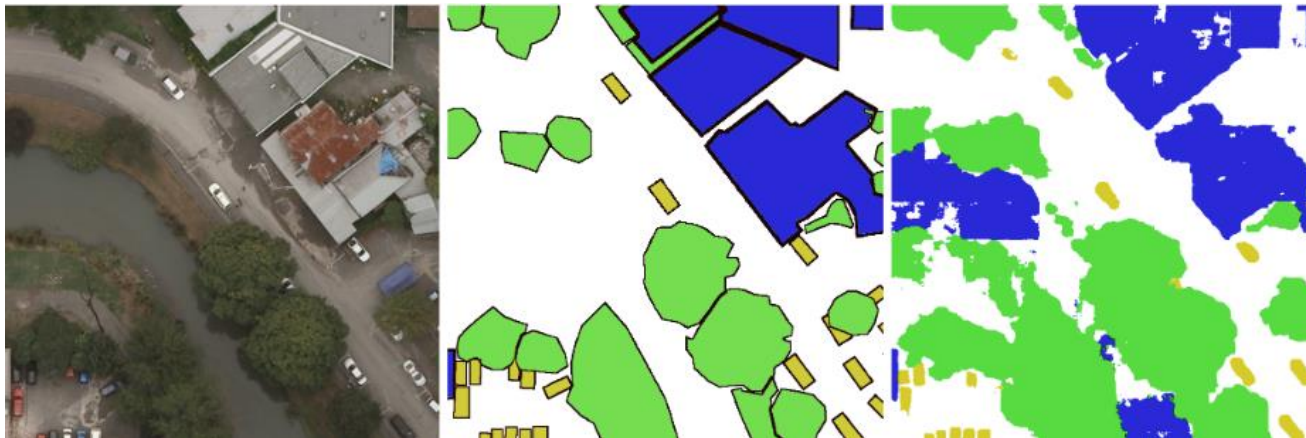
Ballesteros, J.R.; Sanchez-Torres, G.; Branch-Bedoya, J.W. HAGDAVS: Height-Augmented Geo-Located Dataset for Detection and Semantic Segmentation of Vehicles in Drone Aerial Orthomosaics. *Data* **2022**, *7*, 50.

<https://doi.org/10.3390/data7040050>

Related work on automatic vector-object extraction

Point objects segmentation: vehicles

(Audebert et al., 2017) proposed **Segment before Detect** an approach for vehicle segmentation using SegNet over ISPRS Potsdam dataset measured on mIoU.



Line objects segmentation: roads

(Bulatov et al., 2016) **modified Douglas-Peucker algorithm** for street generalization after segmentation and thinning, skeletonization, and filtering. (Gao et al., 2018) presented a **weighted balance loss function** over a **PSPNet** to solve the road class imbalance problem caused by the sparseness of roads. They compared with the **cross-entropy loss function**, and found that it can reduce training time dramatically for the same precision, especially for narrow rural roads.

Related work on automatic vector-object extraction

(Kearney et al., 2020) extracted unpaved roads from RapidEye imagery using a CNN, **hand engineering post-processing improved vector results** that changed the existing roads in 20%.

(Gong et al., 2020) uses a pre-trained VGG network into a U-Net and an attention module to solve road problems like tortuous shape, connectivity, imbalance, occlusion, and different scales. **Then the vector is extracted from the segmentation results** and processed by denoising and straight-line connection and vectorized to realize the automatic road network.

(W. Yang et al., 2021) worked in a method of extracting roads and bridges from high-resolution images, edge detection is performed, and the resultant binary edge is vectorized. Their network integrates **binary cross entropy to deal with road class imbalance**.



Zurbaran et al, 2019

Related work on automatic vector-object extraction

Polygon objects segmentation: buildings

(Sahu & Ohri, 2019) used semantic segmentation model based on **U-Net** to extract buildings using satellite/UAV and dice coefficient ($2 \times \text{IoU}$) and conversion to vectors were performed manually.

(Li et al., 2021) uses the **U-Net**, **Cascade R-CNN**, and **Cascade CNN ensemble** models for building segmentation, building bounding boxes, and building corners, respectively, from very high-resolution images. They later used Delaunay triangulation to construct building footprint polygons based on the detected building corners. The approach has a good performance, but the architecture is too complex and customized.

(Xie et al., 2020) proposes a multifeature convolutional neural network (MFCNN) and morphological filtering, for treating **the irregular building boundaries** resultant from high-resolution images. This method improved IoU by 3.04% respect to normal segmentation.

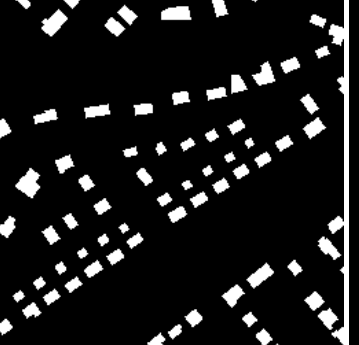
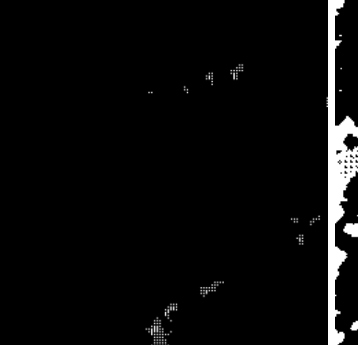
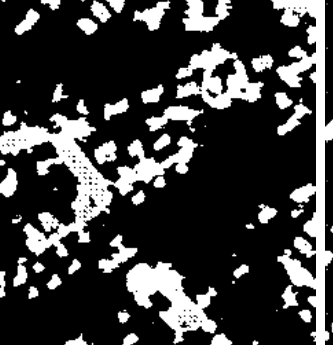
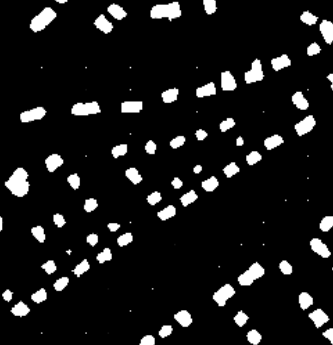


(Sahu & Ohri, 2019)

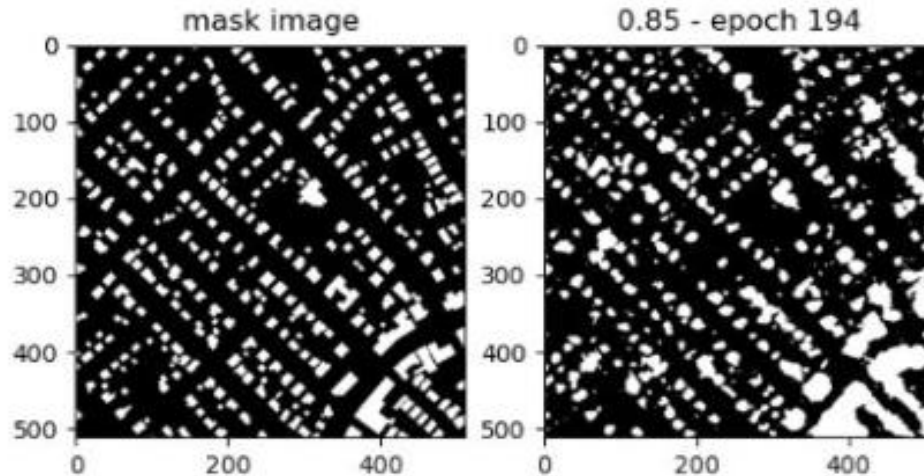
Choosing the Model

Same architecture for point, line, and polygon masks, Class imbalance, Quality masks, Data requirements, Attribute extraction, Cleaning and simplification of masks

Massachusetts Building Dataset, Mnih et al, 2013 100 epochs, 500 images

Aerial Imagery	Label	CvT	Cycle GAN	cGAN	Model	mIoU
					CvT	0.11
					Cycle GAN	0.19
					cGAN	0.79
					U-Net	0.67

CvT, Wu et al, 2021



Pix2Pix cGAN, Isola et al, 2017

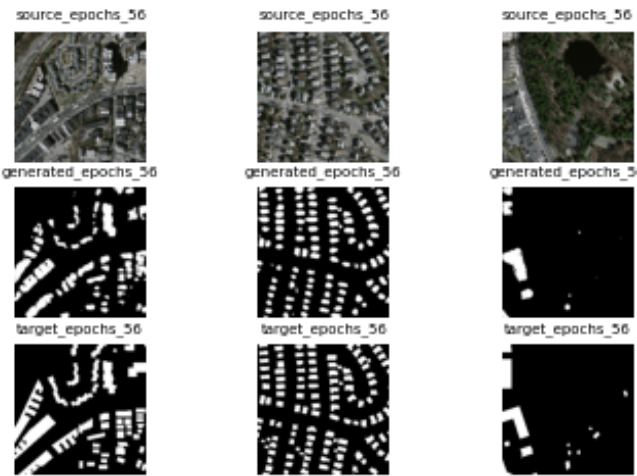
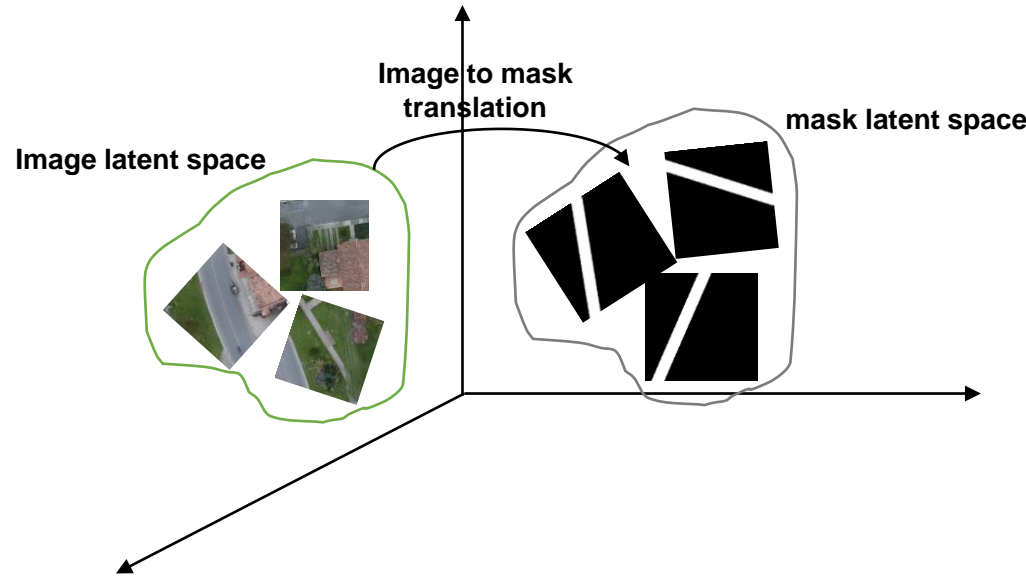
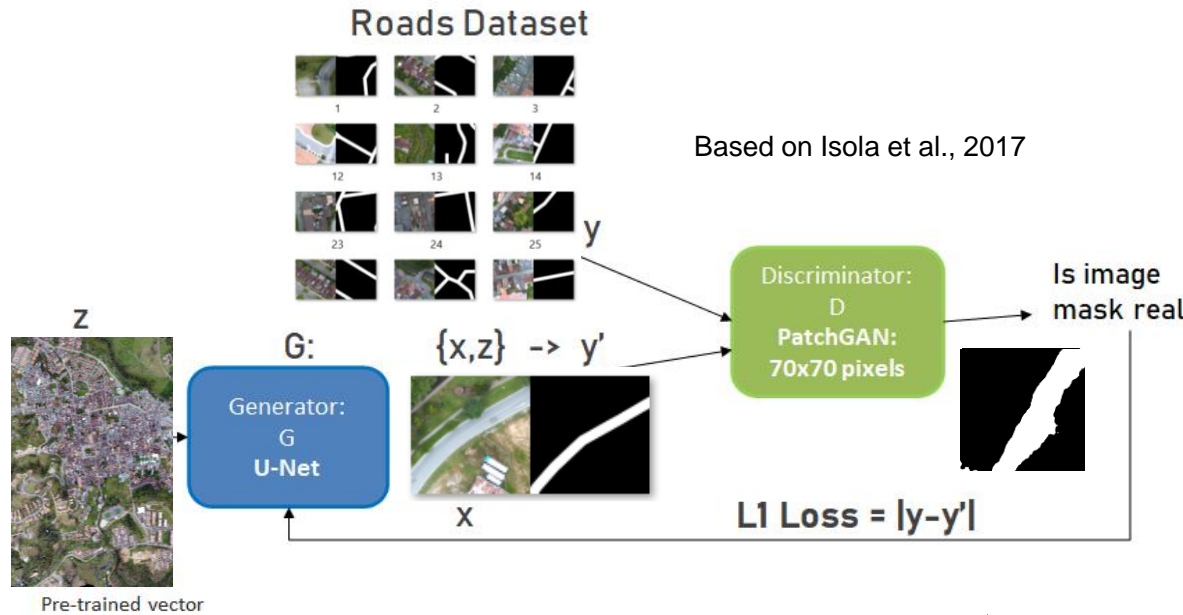


Image to mask translation

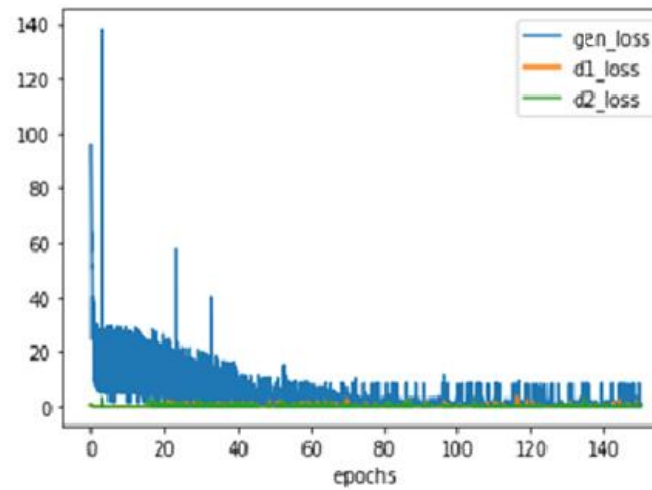


Experiments with the Generative Method

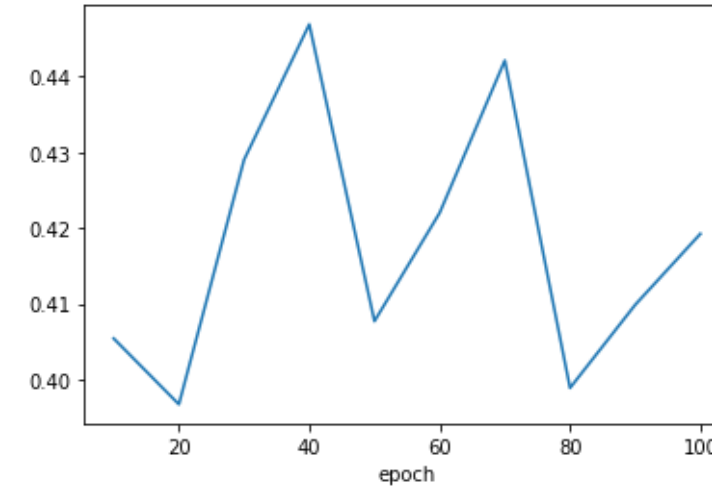
Hyperparameters

Epochs and Batch Size

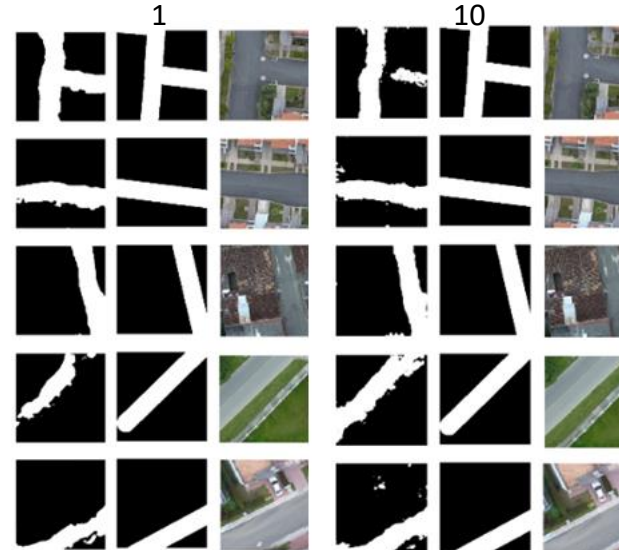
Discriminator and generator losses vs epochs



mIoU vs epochs



Batch size vs mIoU

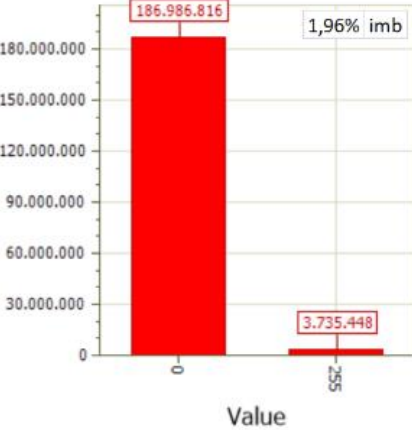


Batch_size	mIoU
1	0.713
10	0.723

Imbalance on the Road Dataset

Imbalance vs buffer distance in roads

Retiro_50cm_roads.tif



Example of a chip of 50 cm

Retiro_1m_roads.tif



These values are averaged for the entire raster masks not yet tessellated.

Retiro_300cm_roads.tif



Example of a chip of 300 cm

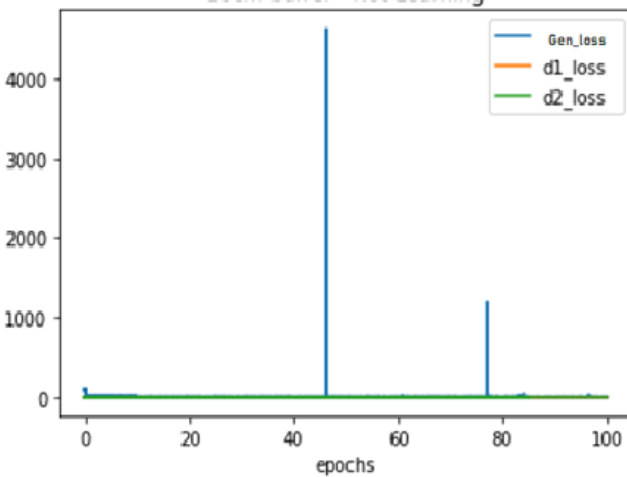
Retiro_500cm_roads.tif



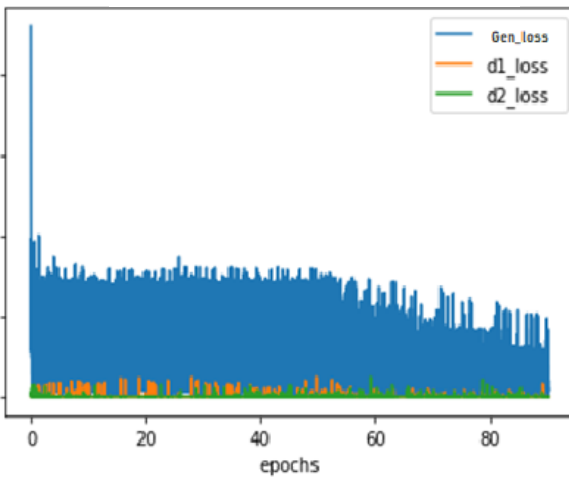
Example of a chip of 500 cm

Effects of Imbalance

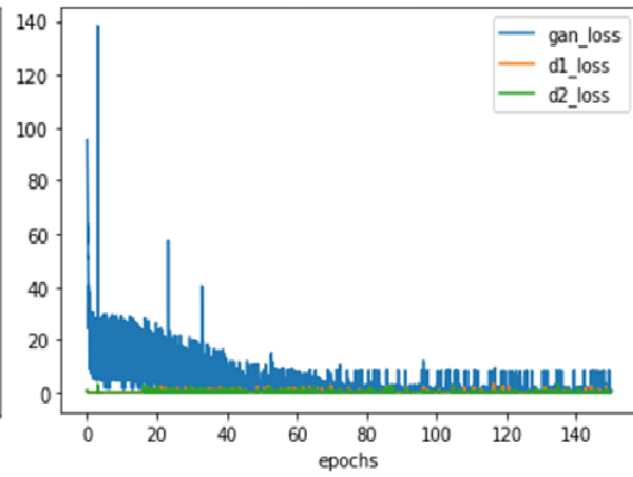
10cm buffer - Not Learning



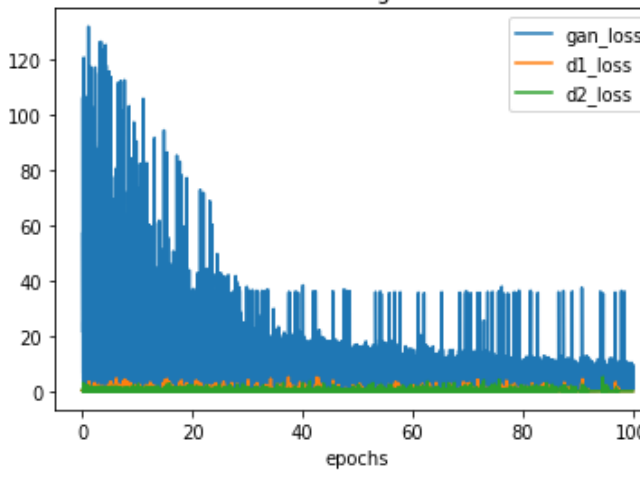
50cm, 7%



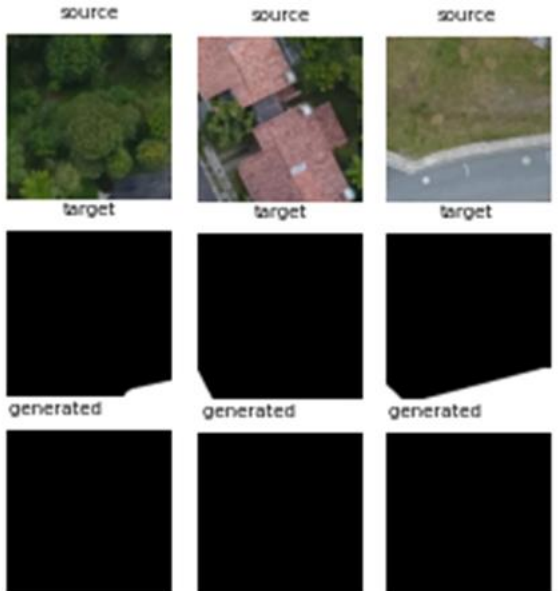
50cm 13.5%



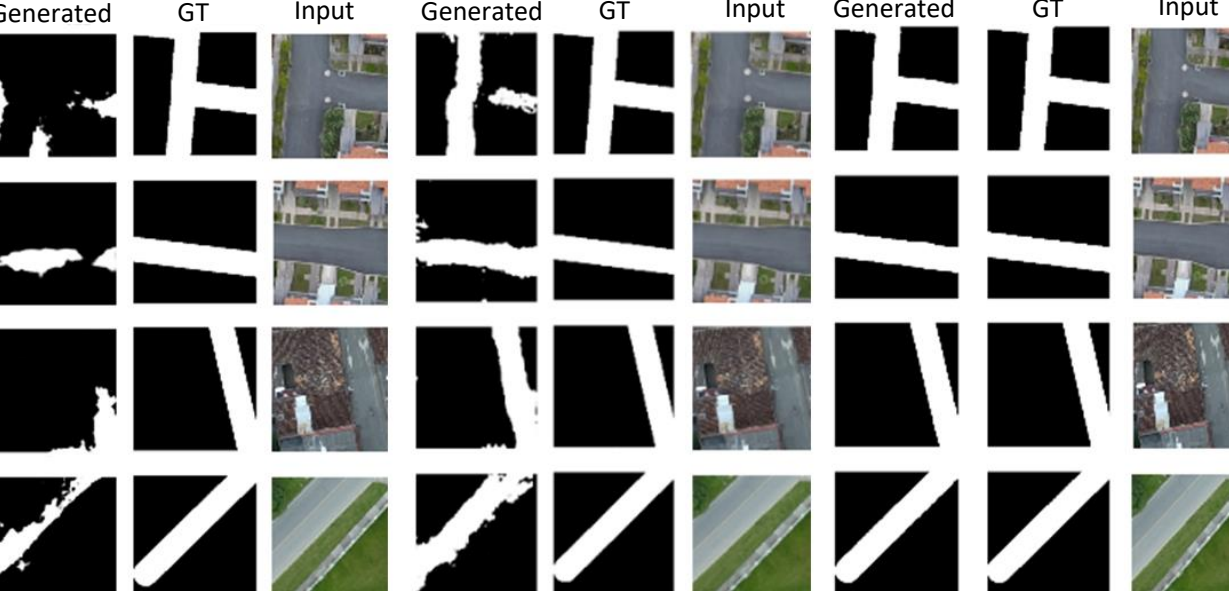
Massachusetts Building Dataset 256x256 16%



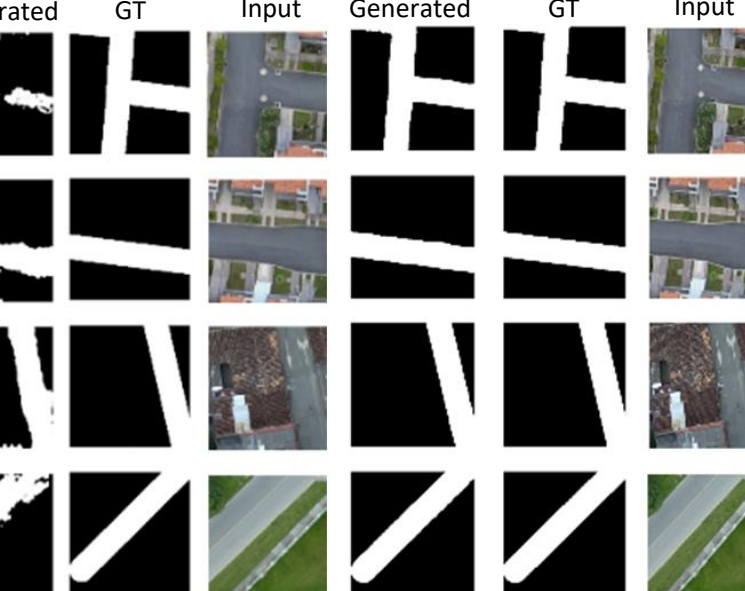
< 1% imbalance



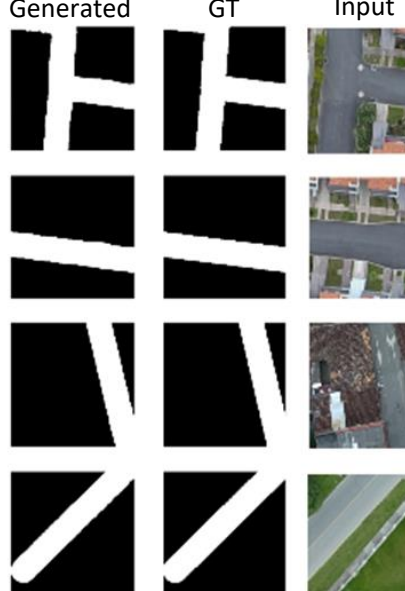
5% imbalance



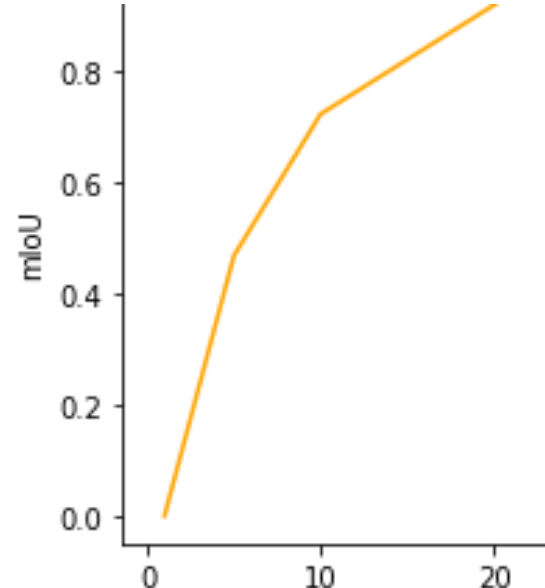
10% imbalance



> 10% imbalance

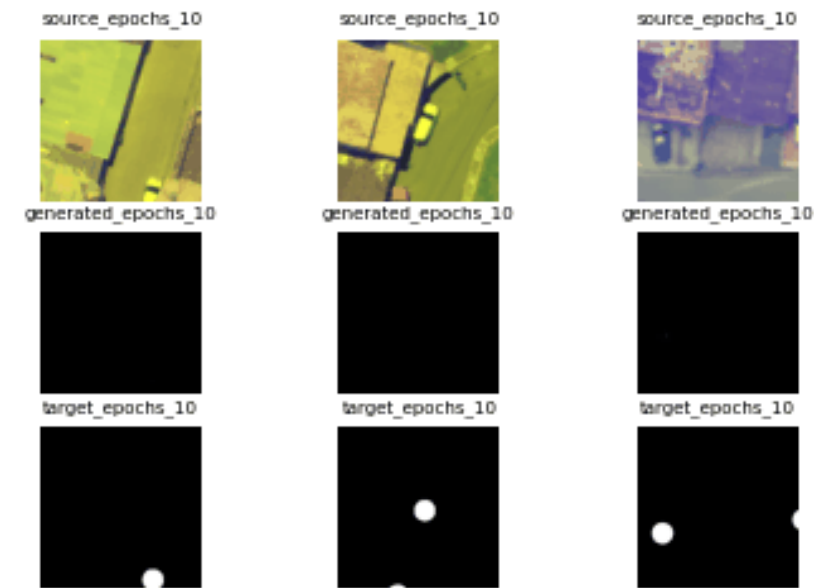


mIoU vs imbalance

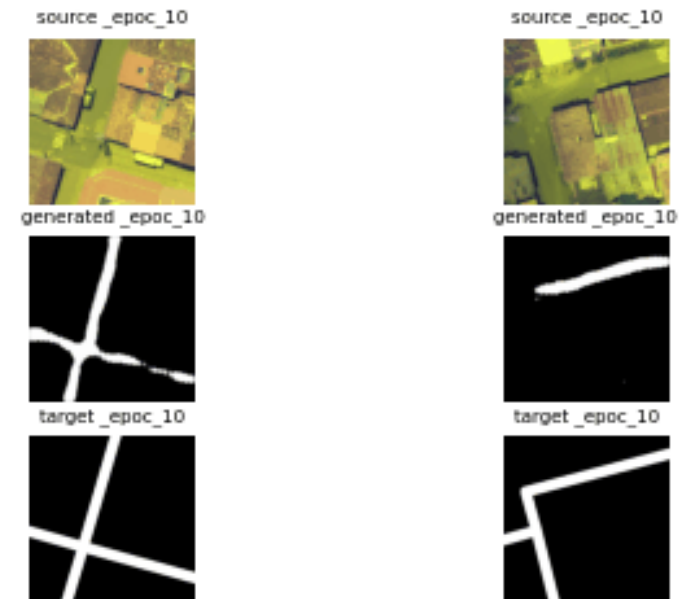


Quality Masks - Examples

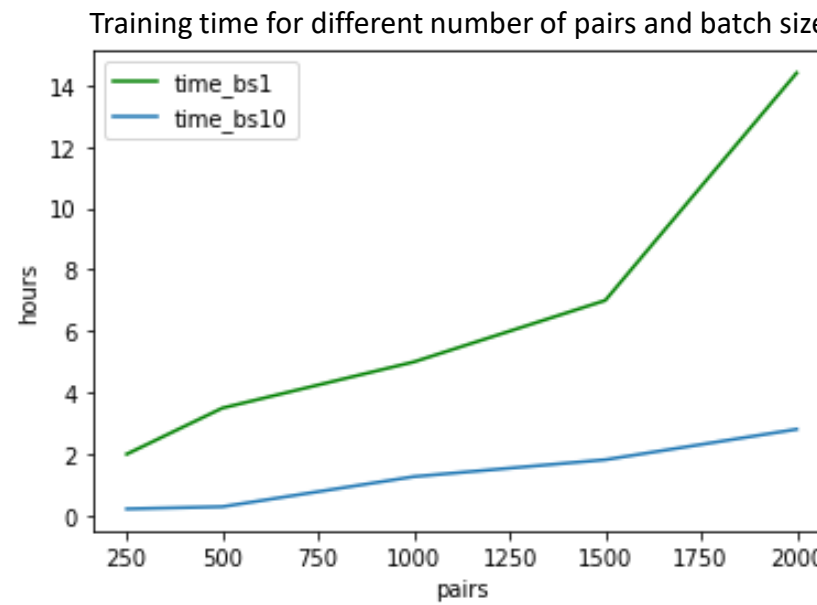
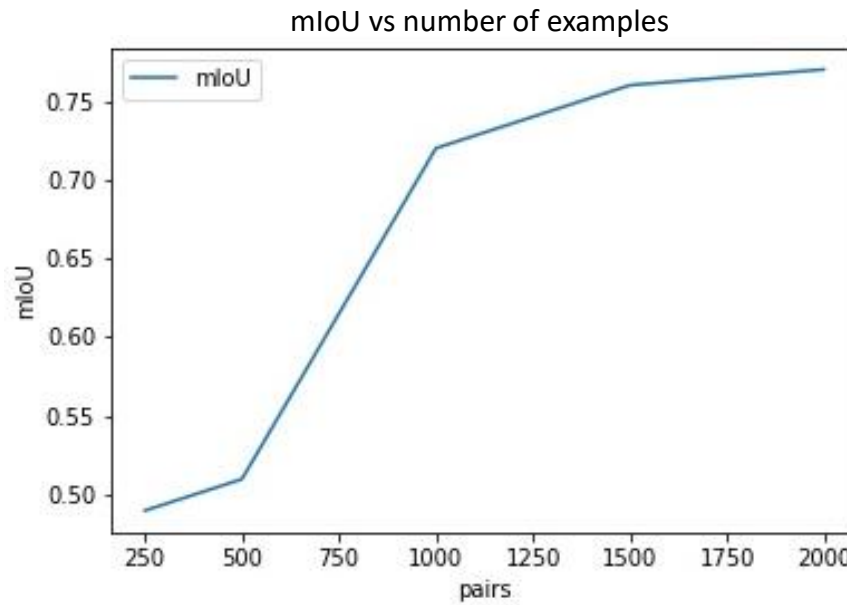
Rain masks, 1,000x1,000m



Testing Road Dataset



Data requirements for linear masks

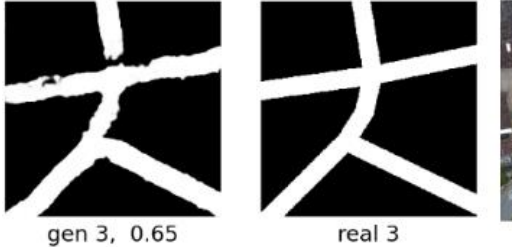
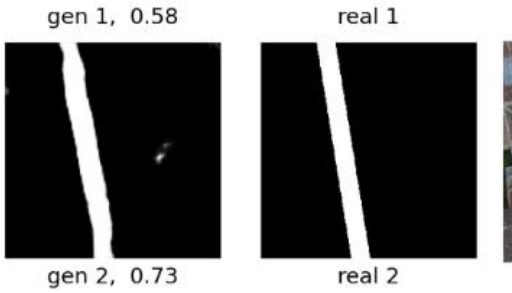


Examples vs pairs in road dataset

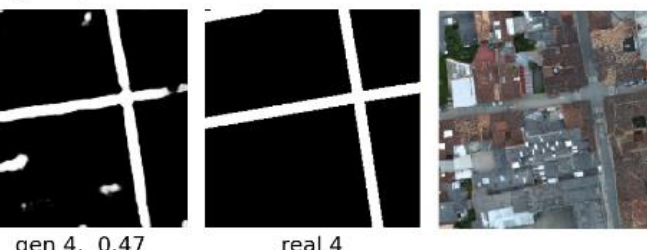
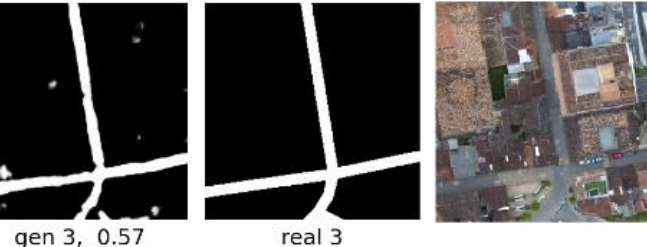
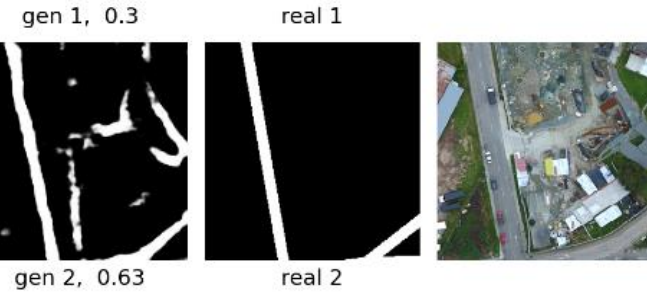
Number of pairs	mIoU
250	0.35-0.48
500	0.49-0.55
1000	0.60-0.72
1500	0.75-0.90
>=2000	>=0.939

Image size for roads

Results using images of 512 x 512 px



Results using images of 1500 x 1500 px



Size vs performance in road dataset

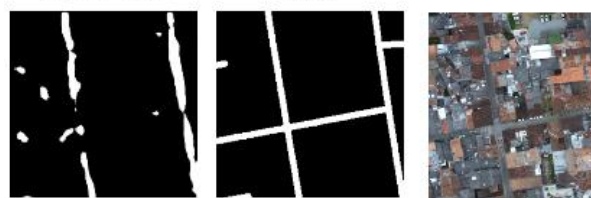
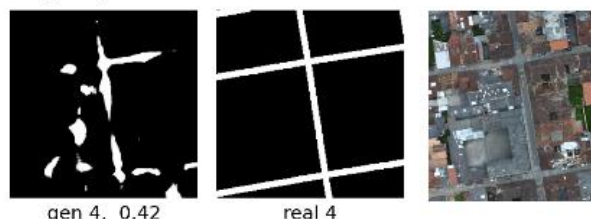
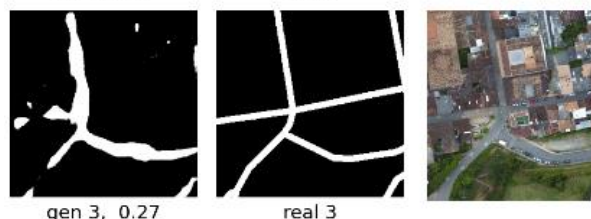
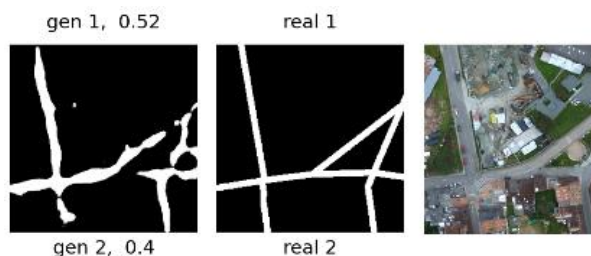
Size (px)	mIoU	Test pairs
256x256	0.53	329
512x512	0.65	378
1024x1024	0.55	329
1500x1500	0.59	329

Multi-scale training

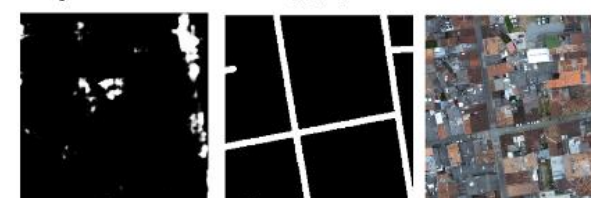
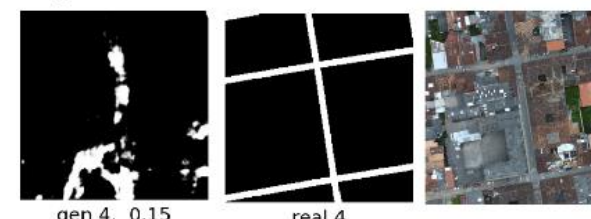
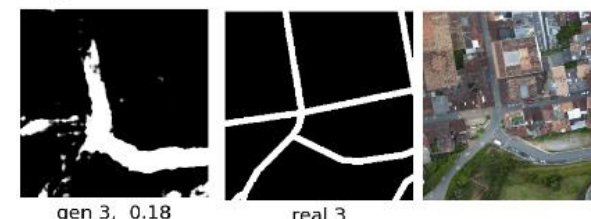
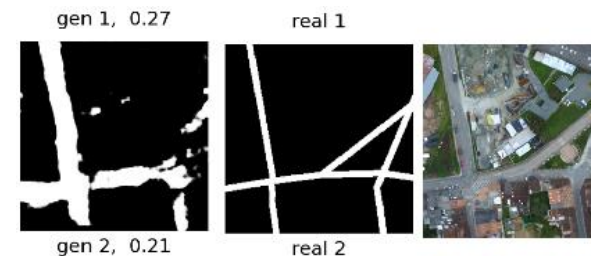
**Bottom-up vs
top-down training**

Size (px)	mIoU	Test pairs
256x256 to 1024x1024	0.40	378
1024x1024 to 256x256	0.28	378
Training at 256 only	0.45	378

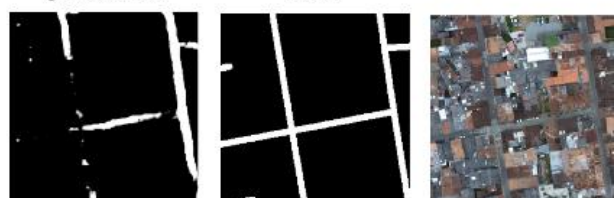
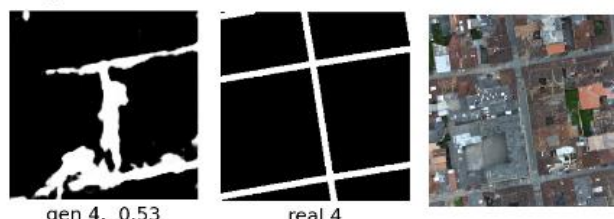
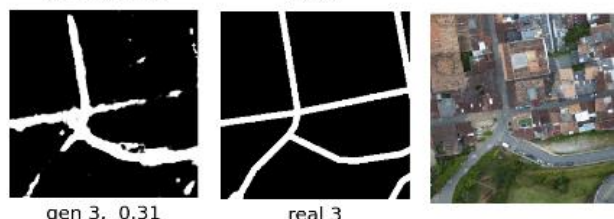
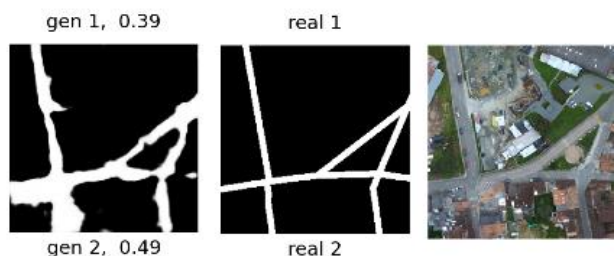
Bottom up Re-training



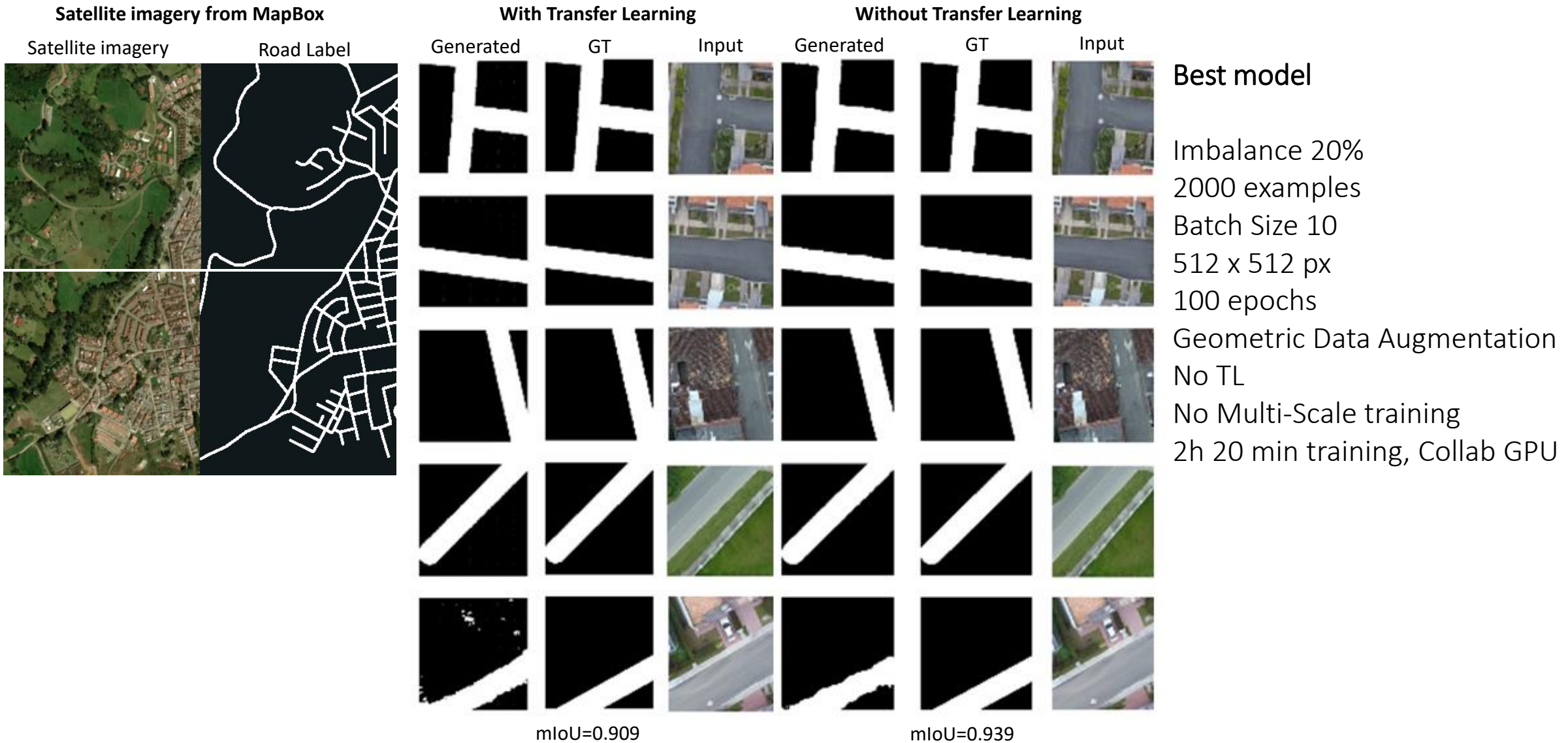
Top down Re-training



256 px only



Transfer Learning and the best model



Data Augmentation

Influence of geometric and spectral augmentation, 500 examples

Augmentation Method	mIoU
Overlapping (30%)	0.794
Mirroring (vert. and hor.)	0.789
Rotation (10 degree increase clockwise)	0.779
Spectral (10% random increase in brightness, intensity and contrast)	0.659
All augmentation together	0.847

30% overlapping



90° mirroring

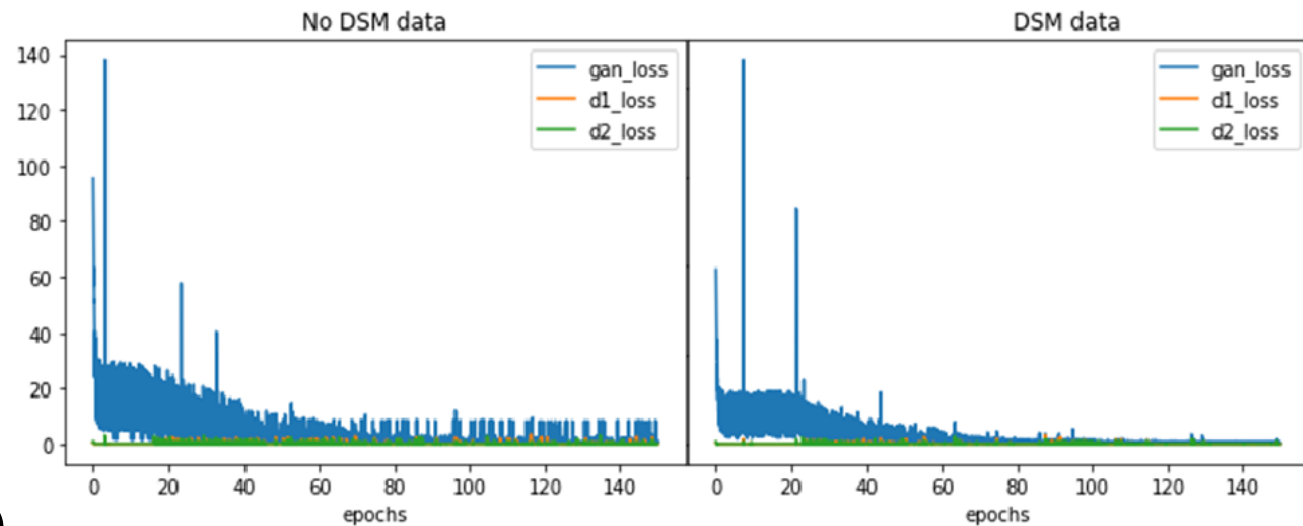


Influence of data fusion, 500 examples

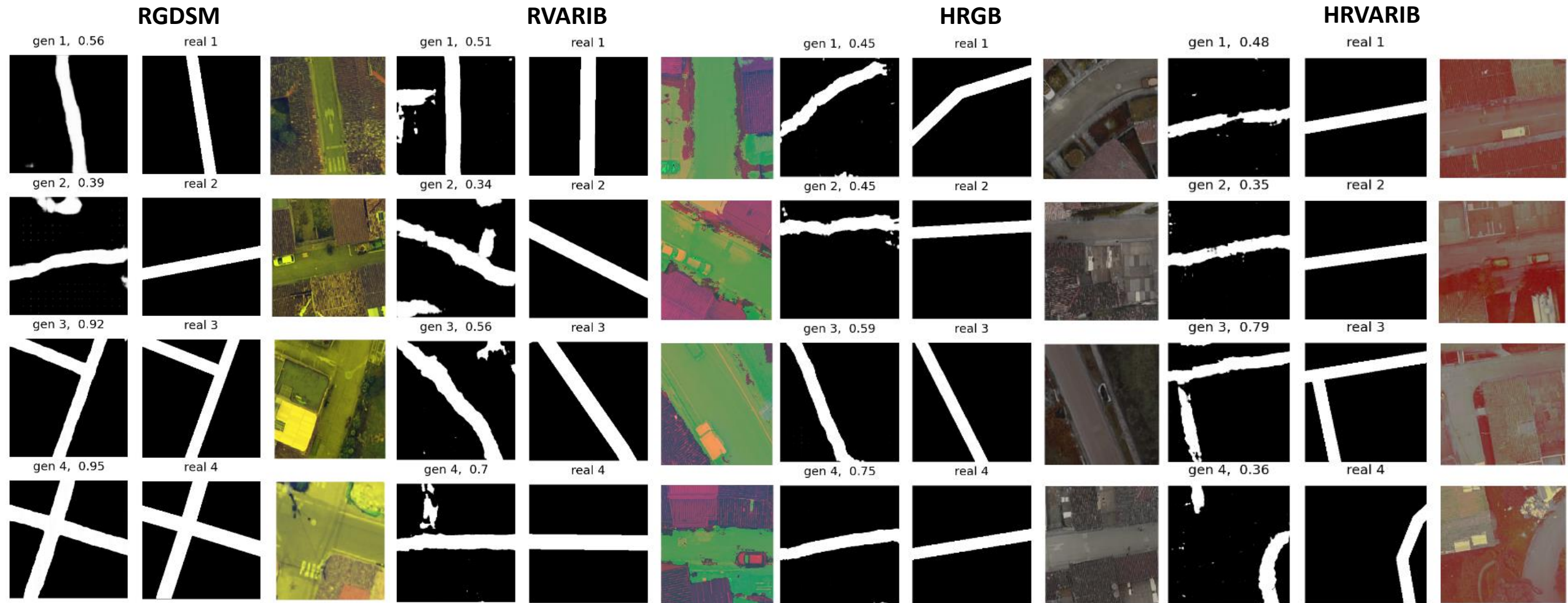
Fusion Method	mIoU
RG-DSM	0.725
RVARIB	0.549
HRGB	0.621
HRVARIB	0.508

$$VARI = (Green - Red) / (Green + Red - Blue)$$

Gitelson et al, 2002



Data Fusion



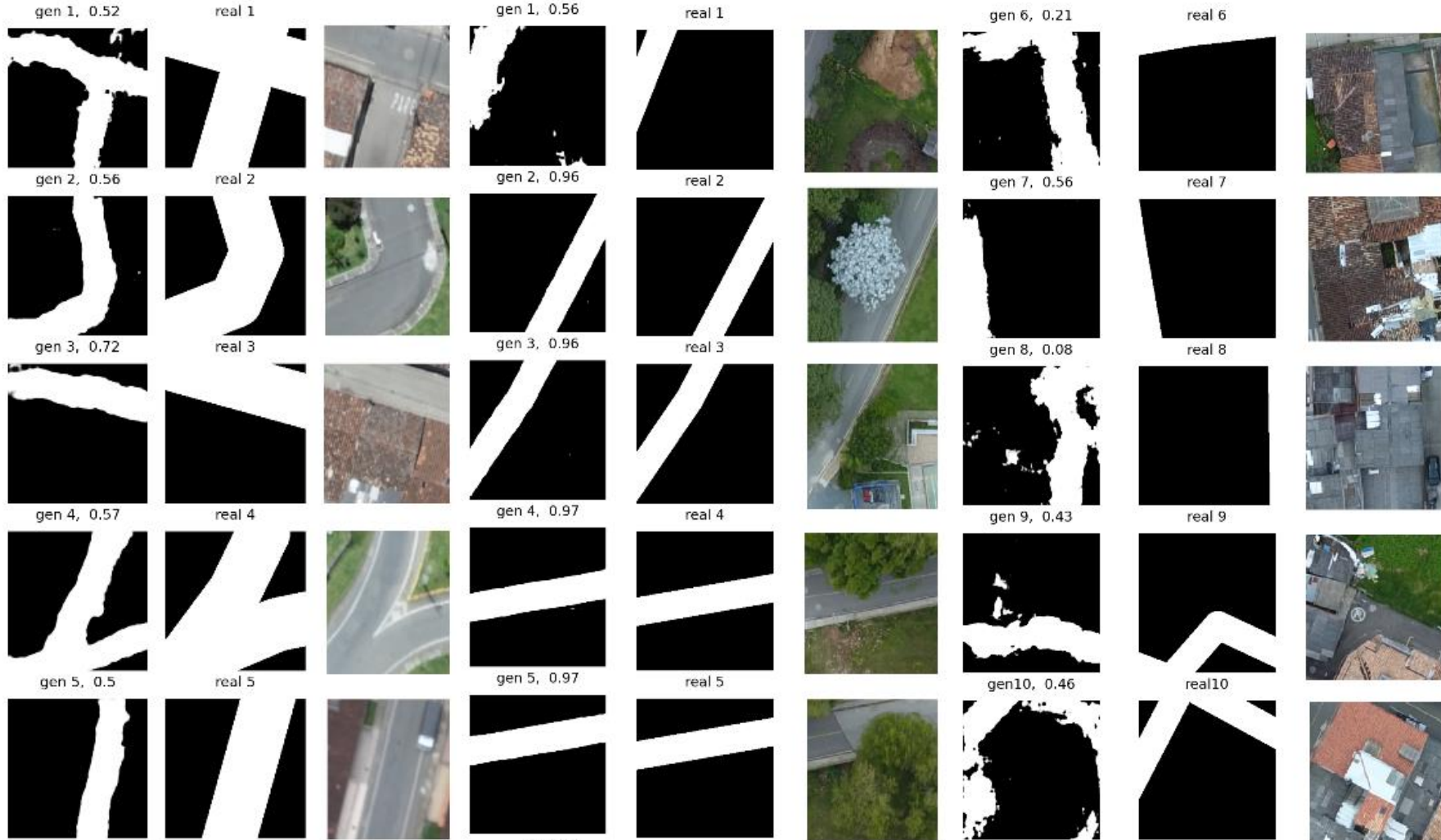
(Zhang et al., 2015) and also (Al-Najjar et al., 2019) combined UAV Ultra-High resolution Orthophotos with DSM to create land cover maps, their experiments demonstrate that the DSM enhanced the results of RGB

Model Generalization

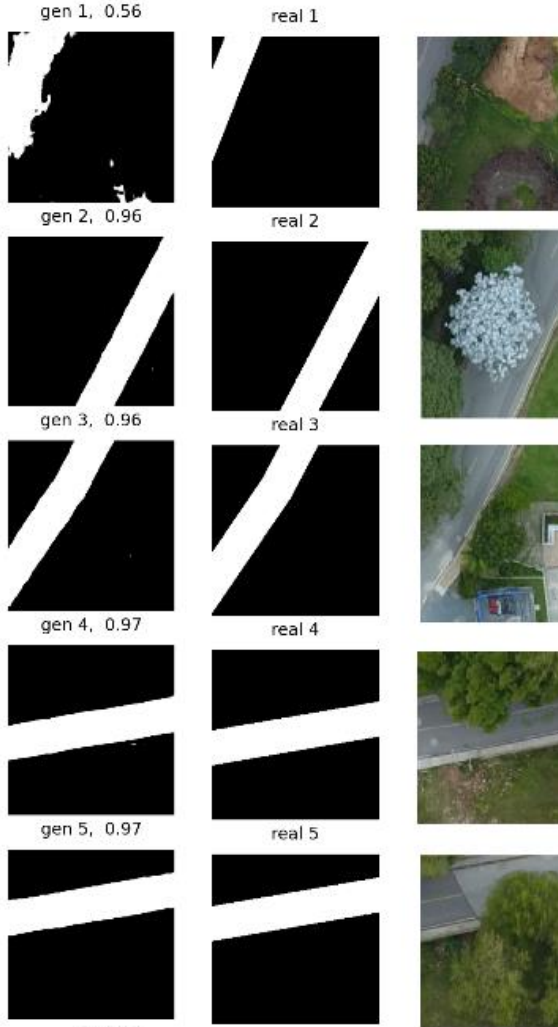
Model Generalization

Case	mIoU
Inferring on different settlements	0.595
Occlusions by trees	0.929
Occlusions by buildings	0.428

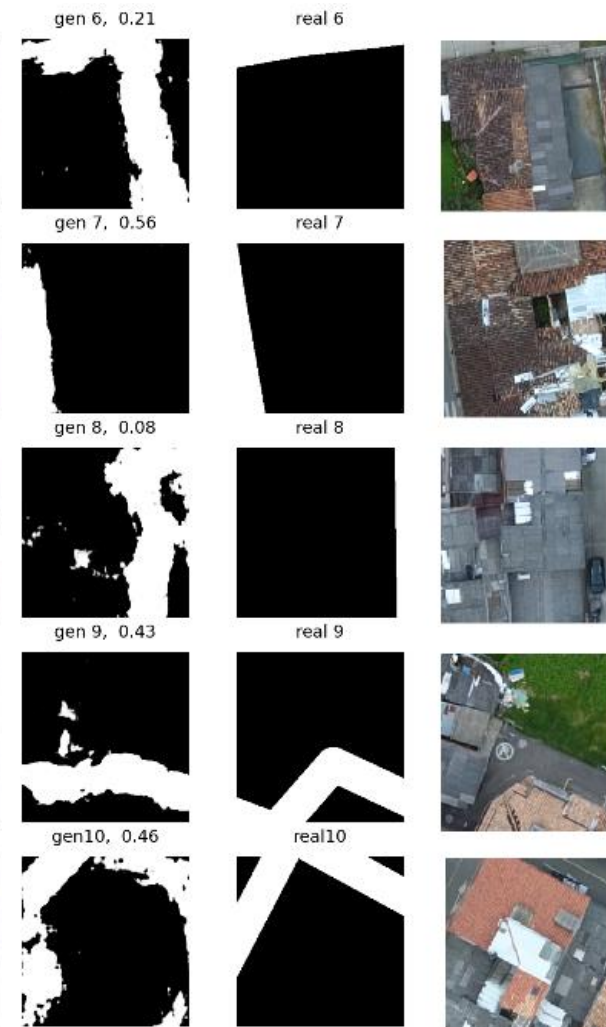
On different settlement



Occlusions by trees

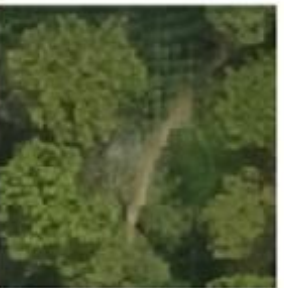
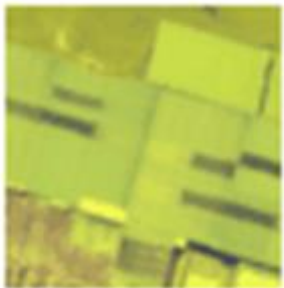


Occlusions by buildings

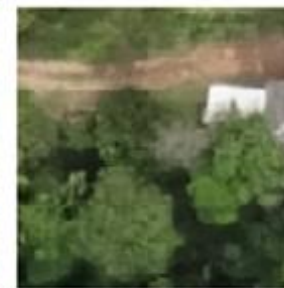


Color decoding for attribute extraction

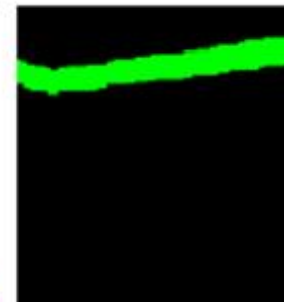
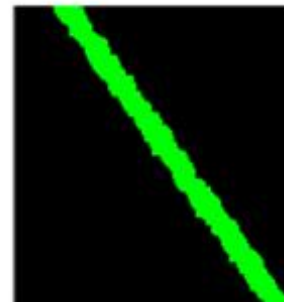
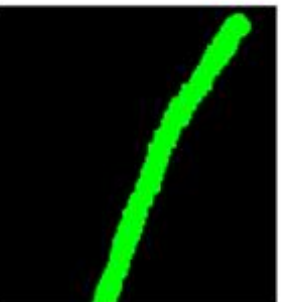
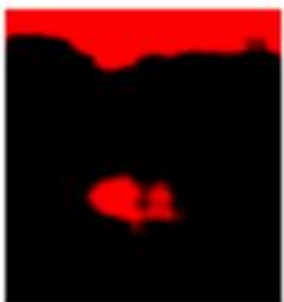
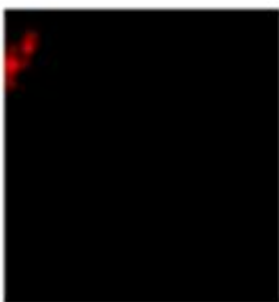
Residential street



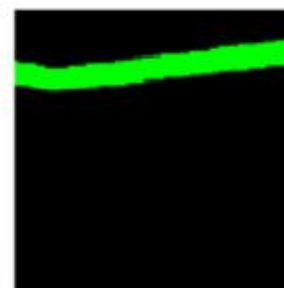
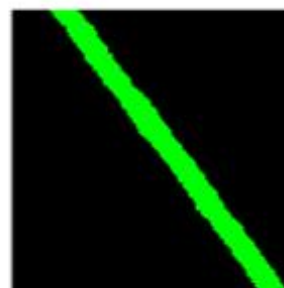
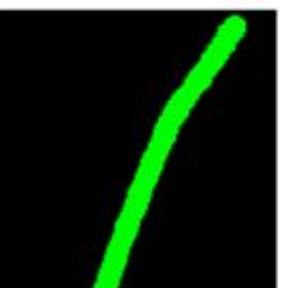
Unpaved road



image



generated

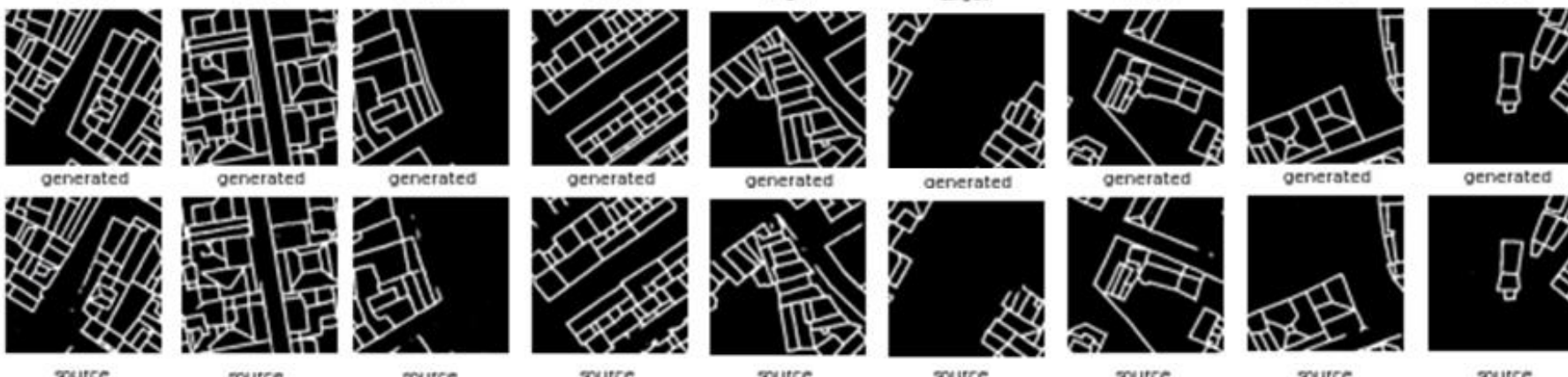


label

mIoU=0.798

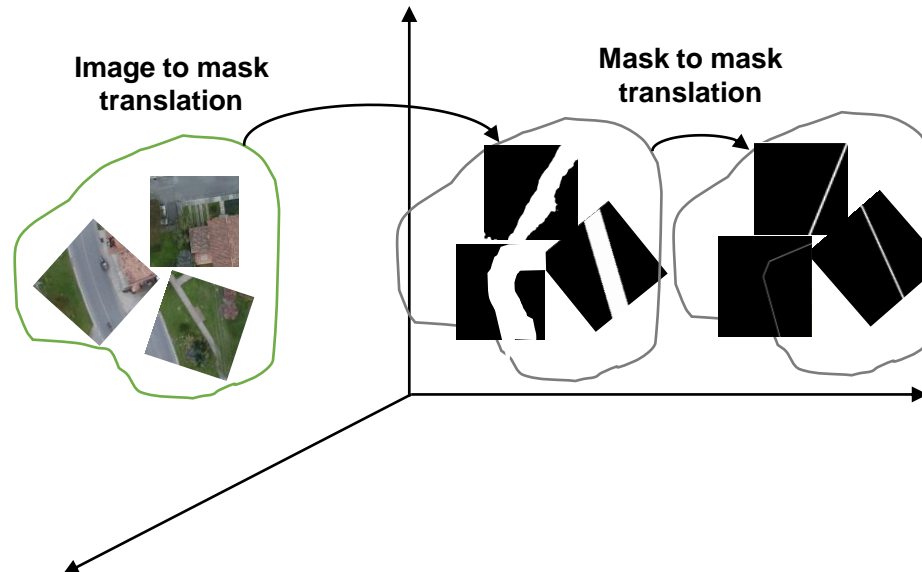
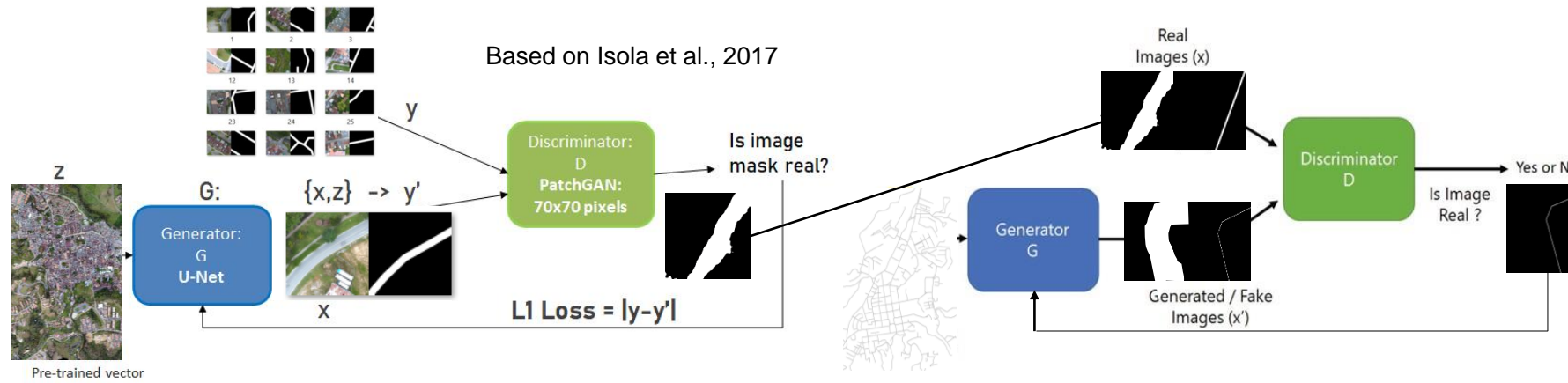
Results on RID: Roof Boundary Mask Dataset

**512x512px
mIoU=0.941**



**256x256px
mIoU=0.950**

Image to mask translation and mask to mask translation



Mask to mask translation and dataset

Both allows to correct spurious masks of roads produced by a DL model.

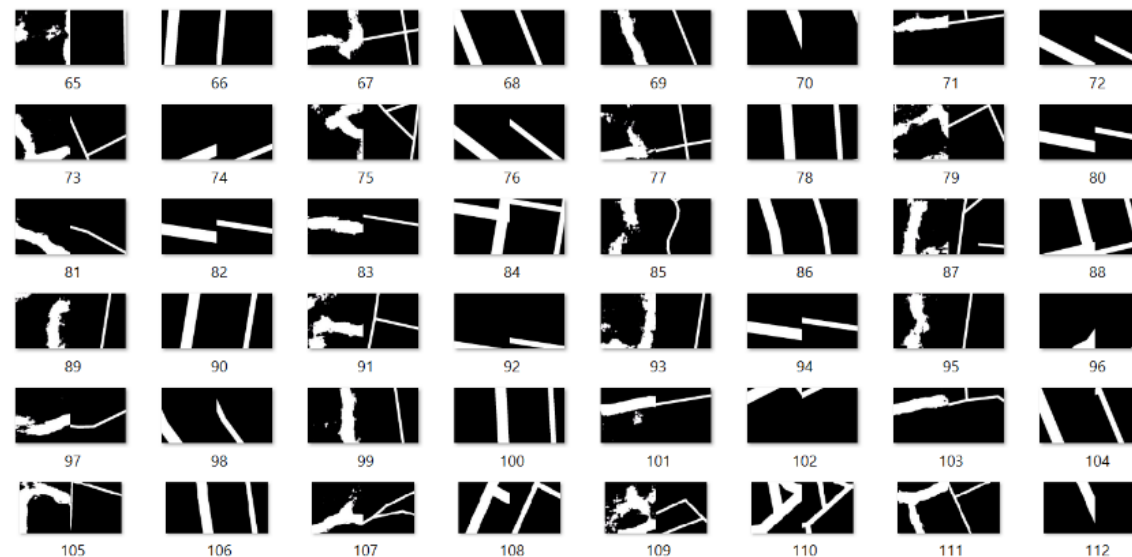
Irregular masks = false positive pixels



Discontinuous masks = false negative pixels

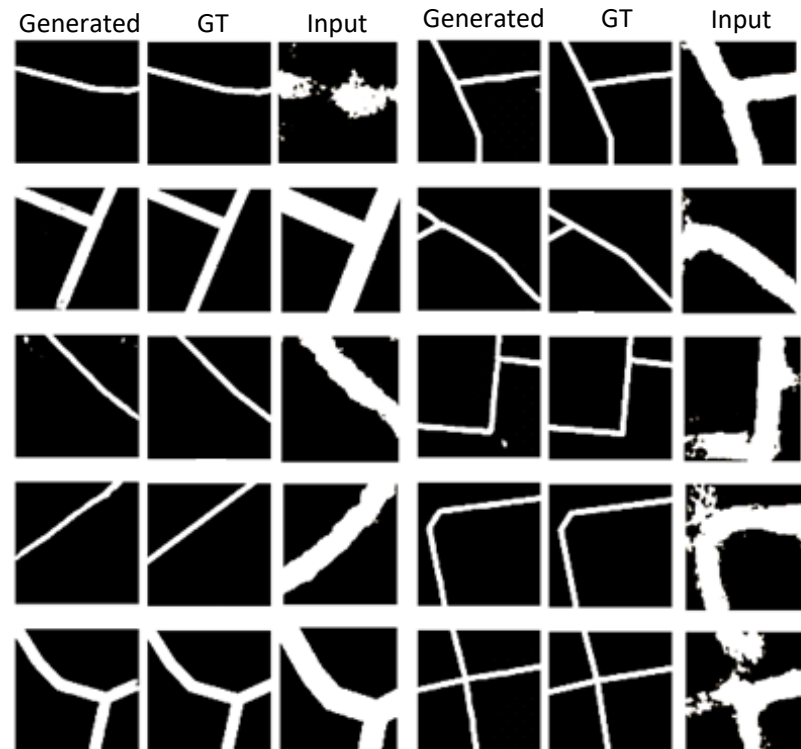


msk2msk dataset



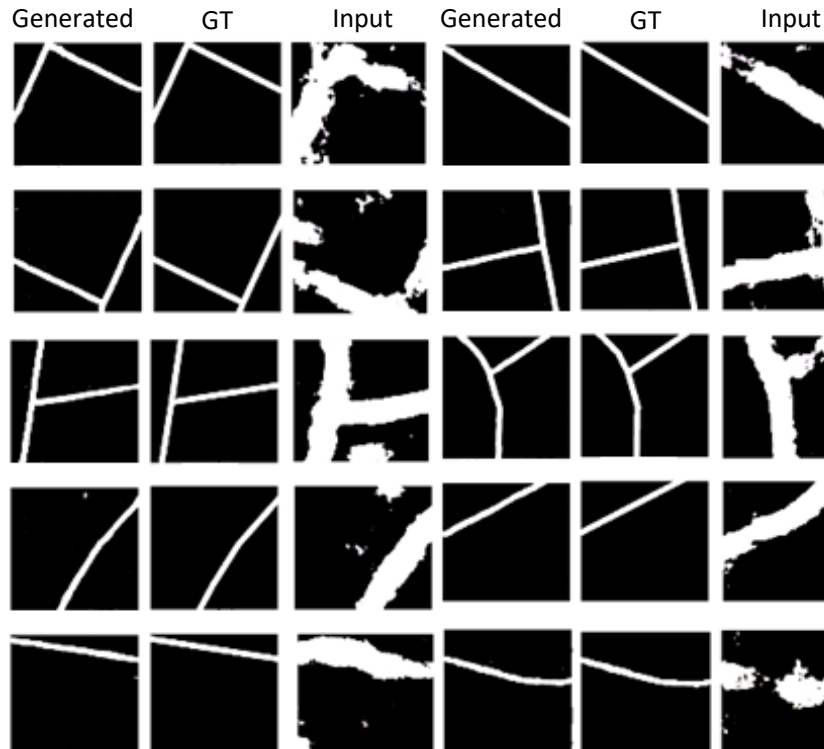
Mask to mask translation

Spurious and clean masks, 500 ex



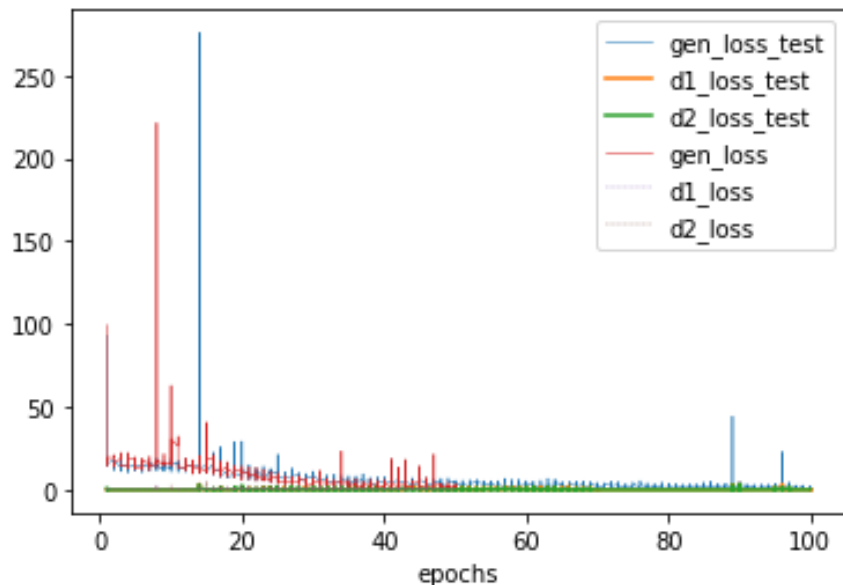
mIoU=0.892

Only irregular and discontinuous spurious masks



mIoU=0.802

Train and test losses



Mask to mask vectorization

Vectorization of a full size mask of a U-Net



Vectorization of a primitive mask 1m after
msk2msk translation

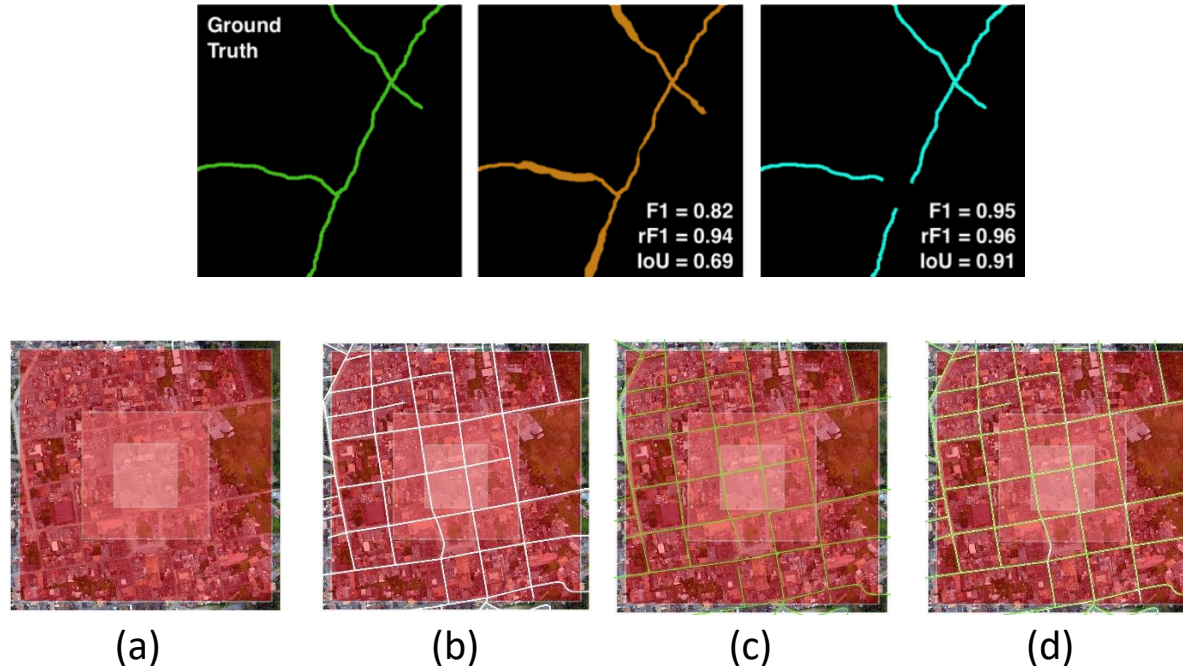


Centerline vector layer



PROPOSED (vector) METRIC: Average Geometry Similarity (AGS)

The Average Path Length Similarity (APLS) (Van Etten et al., SpaceNet, 2019) based upon Dijkstra's shortest path algorithm. sums the differences in optimal paths between GeoJSON vector ground truth and GeoJSON proposal graphs.



$$\text{AGS_Points} = \frac{1}{n} \sum_1^n \left(1 - \min \left\{ 1, \frac{|\#V(a,b) - \#V'(a,b)|}{\#V(a,b)} \right\} \right), \text{ points/s}$$

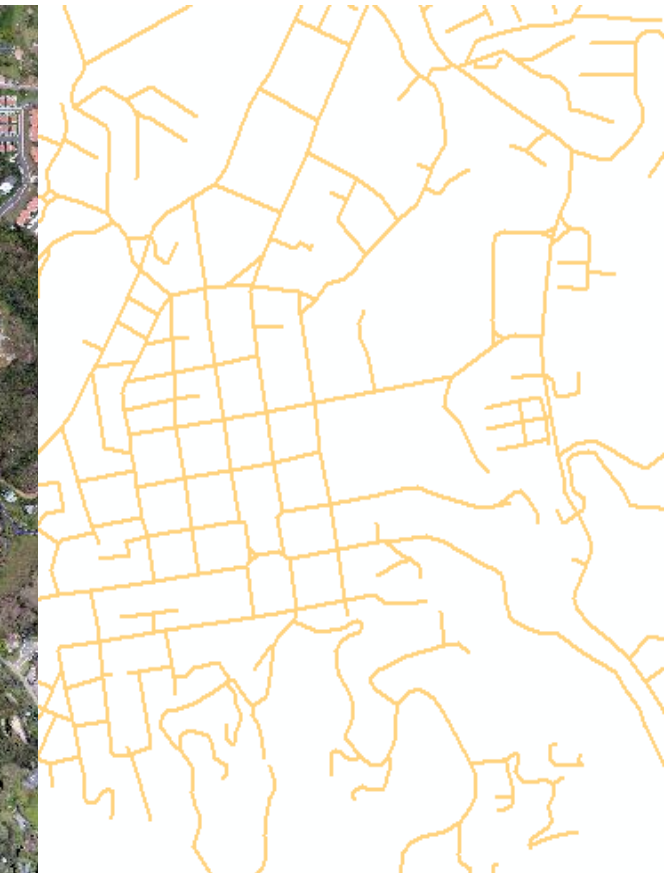
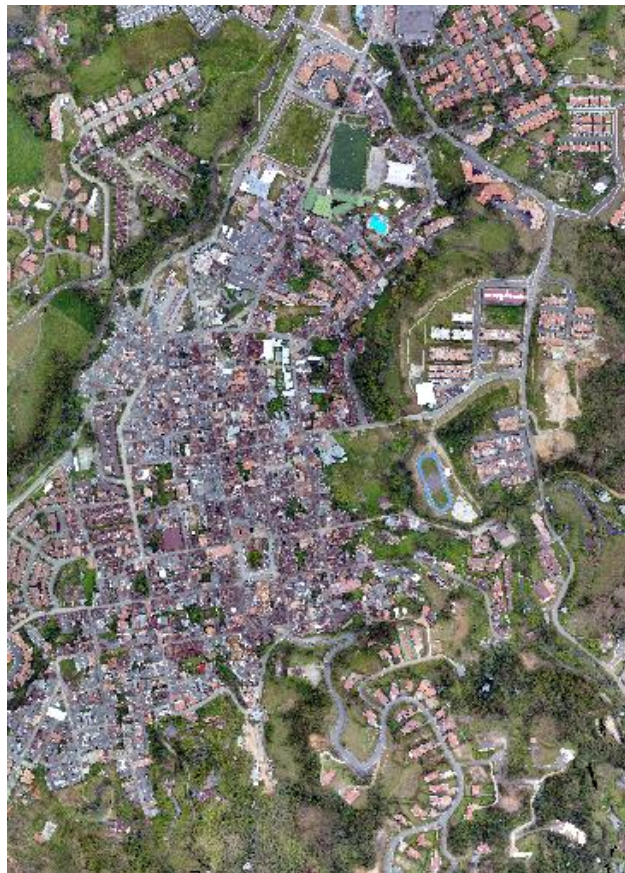
$$\text{AGS_Polygons} = \frac{1}{n} \sum_1^n \left(1 - \min \left\{ 1, \frac{|A(a,b) - A'(a,b)|}{A(a,b)} \right\} \right), \text{ m}^2/\text{s}$$

#V and #V' are the number of points (ie. Vehicles) within an area (a,b)
L and L' are the length of polylines within area (a,b).

AGS RESULTS

Results of estimating AGS_Lines for metric Roads vectorization

Orthomosaic	Application of AGS Metric - Roads	AGS_Lines Collab GPU
El Retiro, (Ant.)	Image to mask translation model and vectorization without primitive masks	0.801 at 12.87 m/s
	Image to mask translation model with primitive masks and vectorization	0.903 at 12.39 m/s
	Model including double image to mask translation and vectorization	0.940 at 12.03 m/s



Ballesteros et al, 2021

Contribution - Papers

- Ballesteros, J.R.; Sanchez-Torres, G.; Branch-Bedoya, J.W. A GIS Pipeline to Produce GeoAI Datasets from Drone Overhead Imagery. *ISPRS Int. J. Geo-Inf.* 2022, **11**, 508. <https://doi.org/10.3390/ijgi11100508>
- Ballesteros, John R.; Sanchez-Torres, German; Branch-Bedoya, John W. HAGDAVS: Height-Augmented Geo-located Dataset for Detection and Semantic Segmentation of Vehicles in Drone Aerial Orthomosaics. *Data*, April 14, 2022, MDPI.
- Ballesteros, J.R.; Sanchez-Torres, G.; Branch, J., Road Semantic Segmentation by Fusion-augmented Drone Orthomosaics using a Conditional GAN. In progress. *Drone*, March 2022, ISPRS Journal of GeoInformation, MDPI. In Reviewing.
- Ballesteros, J.R.; Sanchez-Torres, G.; Branch, J., Mask-to-Mask Translation Generative Model for Improving Roads and Buildings Segmentation in Drone Overhead Imagery. In progress. *Drone*, March 2022, ISPRS Journal of GeoInformation, MDPI. In Reviewing.
- Ballesteros, J.R.; Sanchez-Torres, G.; Branch, J., Extracting Building Roof Structure of Dense Areas using a cGAN and a Boundary Mask Dataset. In progress. *Drone*, March 2022, ISPRS Journal of GeoInformation, MDPI. In Reviewing.

Contribution - Conferences

- Ballesteros John, Branch-Bedoya John W., Sánchez-Torres Germán. Automatic road extraction in small urban areas of developing countries. The IEEE SCLA International Conference 2021.
- Ballesteros John, Branch-Bedoya John W., Sánchez-Torres Germán. Semantic Segmentation of Urban objects in Satellite and Drone Imagery using Deep Learning. International Conference on Civil Engineering, Concivil 2022.
- Ballesteros John, Sánchez Germán, Branch John. Modelo de generación automática de capas SIG a partir de aprendizaje profundo. Congreso Colombiano de Geología. Medellín, Agosto 2021.

References

- 1. Abdollahi, Abolfazl & Pradhan, Biswajeet & Shukla, Nagesh & Chakraborty, Subrata & Alamri, Abdullah. (2020). Deep Learning Approaches Applied to Remote Sensing Datasets for Road Extraction: A State-Of-The-Art Review. *Remote Sensing*. 12. 1444. 10.3390/rs12091444.
- 2. Adam Van Etten, Dave Lindenbaum, Todd Bacastow. SpaceNet: A Remote Sensing Dataset and Challenge Series. *Computer Vision*. 2019.
- 3. Alec Radford, et al. “Unsupervised Representation Learning with Deep Convolutional Generative Adversarial Networks”. ICLR 2016.
- 4. Al-Najjar, H.A.H.; Kalantar, B.; Pradhan, B.; Saeidi, V.; Halin, A.A.; Ueda, N.; Mansor, S. Land Cover Classification from fused DSM and UAV Images Using Convolutional Neural Networks. *Remote Sens*. 2019, 11, 1461. <https://doi.org/10.3390/rs11121461>
- 5. Arnadi Murtiyoso, Mirza Veriandi, Deni Suwardhi, Budhy Soeksmantono and Agung Budi Harto. Automatic Workflow for Roof Extraction and Generation of 3D CityGML Models from Low-Cost UAV Image-Derived Point Clouds. *International Journal of Geo-Information*, 2020.
- 6. Batra et al. Improved Road Connectivity by Joint Learning of Orientation and Segmentation. *CVPR* 2019.
- 7. Brownlee J. www.machinelearningmastery.com (accessed on 12 March 2020).
- 8. Bulatov, Dimitri & Häufel, Gisela & Böge, Melanie. (2016). VECTORIZATION OF ROAD DATA EXTRACTED FROM AERIAL AND UAV IMAGERY. ISPRS - International Archives of the Photogrammetry, Remote Sensing and Spatial Information Sciences. XLI-B3. 567-574. 10.5194/isprs-archives-XLI-B3-567-44

Referencias (Cont.)

- 10. Crommelinck, Sophie & Bennett, Rohan & Gerke, Markus & Nex, Francesco & Yang, Michael Ying & Vosselman, George. (2016). Review of Automatic Feature Extraction from High-Resolution Optical Sensor Data for UAV-Based Cadastral Mapping. *Remote Sensing*. 8. 689. 10.3390/rs8080689.
- 11. Danyang Cao, Zhixin Chen, and Lei Gao. (2020). An improved object detection algorithm based on multi-scaled and deformable convolutional neural networks. *Human Centric Computing Information Sciences*. (2020). Available online: <https://doi.org/10.1186/s13673-020-00219-9>
- 12. Demir et al. DeepGlobe 2018: A Challenge to Parse the Earth through Satellite Images. *CVPR* 2018.
- 13. D. Marmanisa,c, K. Schindlerb , J. D. Wegnerb , S. Gallianib, M. Datcua , U. Stillac. Classification with an edge: improving semantic image segmentation with boundary detection. Elsevier, 2018.
- 14. Eberhard Gülich. Digital systems for automated cartographic feature extraction. Institute of Photogrammetry, University of Bonn. *International Archives of Photogrammetry and Remote Sensing*. 2000.
- 15. Fetaj, Bujar & Oštir, Krištof & Fras, Mojca & Lisec, Anka. (2019). Extraction of Visible Boundaries for Cadastral Mapping Based on UAV Imagery. *Remote Sensing*. 11. 1510. 10.3390/rs11131510.
- 16. Haihong Li. Semi-automatic road extraction from satellite and aerial images. Doctoral Thesis. Swiss Federal Institute of Technology Zurich. 1997. Available online: <https://doi.org/10.3929/ethz-a-001766570>, (accessed on 21 November 2020).

Referencias (Cont.)

- 18. Howard J. <https://course.fast.ai/part2> (accessed on 19 April 2021).
- 19. Hsiuhan Lexie Yang, Jiangye Yuan, Dalton Lunga, Melanie Laverdiere, Amy Rose, Budhendra Bhaduri. Building Extraction at Scale using Convolutional Neural Network: Mapping of the United States. *IEEE Journal of Selected Topics in Applied Earth Observations and Remote Sensing* (Volume: 11, Issue: 8, Aug. 2018).
- 20. Hui Yang, Penghai Wu, Xuedong Yao, Yanlan Wu, Biao Wang, and Yongyang Xu. Building Extraction in Very High Resolution Imagery by Dense-Attention Networks. *Remote Sensing*, 2018.
- 21. Ian Goodfellow, Yoshua Bengio and Aaron Courville. Deep Learning. MIT Press, 2016. Available online: <http://www.deeplearningbook.org>, (accessed on 16 April 2021).
- 22. Ian J. Goodfellow, Jean Pouget-Abadie, Mehdi Mirza, Bing Xu, David Warde-Farley, Sherjil Ozair, Aaron Courville, Yoshua Bengio. Generative Adversarial Networks. NIPS 2014: 2672-2680.
- 23. Jiangye Yuan. Learning Building Extraction in Aerial Scenes Using Convolutional Networks. *IEEE Transactions on Pattern Analysis and Machine Intelligence* (Volume: 40, Issue: 11, Nov. 1 2018).
- 24. Jennings Anderson, Dipto Sarkar and Leysia Palen. (2019). Corporate Editors in the Evolving Landscape of OpenStreetMap. *International Journal of Geo Information*, 2019.